A Study on the Fabrication and Application of Copper Oxide Nanowires Based on Stress-induced Method

Yumei YUE

A Study on the Fabrication and Application of Copper Oxide Nanowires Based on Stress-induced Method

Yumei YUE (岳玉梅)

Department of Mechanical Science and Engineering, Nagoya University

February 2012

ABSTRACT

The large-scale and high-quality aligned Cu_2O nanowires fabricated uniformly on the SiO_2/Si substrate are studied in this dissertation by the stress-induced method. The stress-induced method provides simple, time-saving, economic, and environmentally friendly performance in Cu_2O nanowires fabrication even without the help of any templates and catalysts. The novel process is verified of importance and significance by studying the results of X-ray diffraction (XRD) and transmission electron microscopy (TEM) on samples. It is found that nanowires growing on the substrate are mainly composed of CuO by the direct cooling process, while nanowires growing on the hillocks are mainly composed of Cu_2O by the gradual cooling process. The significance of the gradual cooling process in fabricating Cu_2O nanowires is first proposed. Here, the creative nanowire growth procedure of the method is demonstrated. The high-quality Cu_2O nanowires with aspect ratio up to 300 and growth density higher than $10^9/cm^2$ have been developed under the optimum growth condition of cooling gradually for 4 hours after heating for 5 hours at temperature of 340°C. The as-obtained Cu_2O nanowires are mainly single-crystal ones with smooth surfaces and uniform cross-sections along their axes.

Continued development of Cu_2O nanowire-based electronic and optoelectronic devices requires the ability to tightly control the physical properties of nanowires including diameter and aspect ratio. Adjusting the thickness of the deposited Cu film is concluded to be the optimal way to fabricate Cu_2O nanowires with different diameters. Taking into

account that the length of the as-obtained Cu_2O nanowires is mainly dependent on the heating time, the proper management of Cu film thickness and heating time can give rise to Cu_2O nanowires with controllable diameters and aspect ratios. Dependable parameter control offers a huge advantage in manufacturing Cu_2O nanowires for application in many fields.

The systematic study in this dissertation makes possible the overall understanding of nanowire fabrication and hillock growth. A new stress-redistribution phenomenon related to the cooling process has also been found and explained in detail.

In practical application, the control of nanowire position in a specific integrated device should be designed. The photolithography technique has been developed to aid position control of copper oxide nanowire growth with designed patterns. The study of position control of nanowires plays a key role in the future applications in nanotechnology.

Moreover, the photovoltaic application of Cu_2O nanowires has been presented, which further provides a direct method to develop low-cost solar cell. The as-obtained Cu_2O nanowires on hillocks with high surface areas can absorb more light when they are used as part of a solar cell, which indicates Cu_2O nanowires on hillocks are good candidates for use in photovoltaic application. The typical photovoltaic effect found in the Cu_2O/Cu multilayer structure makes it a potential option for cheap and low toxicity photovoltaic devices with good environmental acceptability. Although the overall performance of the photovoltaic effect is not optimized yet, the study of photovoltaic effect may arouse further economic and convenient methodologies to fabricate practical nanowire-based devices and pave the way for developing new-style solar cell.

The research in this dissertation sets a foundation from nanowire fabrication to possibilities for various kinds of applications. Additionally, the method has a future in fabrication of other metal materials.

Key words:

Nanowires, Nanostructure, Stress-induced method, Thin films, Diffusion, Cooling process, Heating process, Photovoltaic effect, Controllable diameter

CONTENTS

Page

Chapter 1 Introduction

1.1 Background and Motivation

Nanotechnology, which can be defined as the creation and utilization of materials, devices, and systems through the control of matter on the nanometer-scale, has been an exciting and rapidly expanding area of research for more than a decade, and it is also experiencing a flourishing development in a variety of fields.[1, 2, 3] Phenomena at the nanometer scale expose a completely new world， and the properties of matter at the nanoscale are not as predictable as those observed at larger dimensions. Important changes in behavior are caused not only by the continuous modification of characteristics with diminishing size, but also by the emergence of totally new traits. For example, the color of light emitting from semiconductor nanoparticles varies with their sizes;[4] the melting temperature of gold nanoparticles drops dramatically when their size is lower than 20 nm.[5] Nanotechnology is also promoting the unprecedented understanding of materials and devices and impacts many fields. All natural materials and systems establish their foundation at the nanoscale. Therefore controlling matter at the atomic or molecular levels means tailoring fundamental properties, phenomena, and processes exactly at the scale where basic properties are initiated. Nanotechnology could impact the production of virtually every human-made object – from automobiles and electronics to

advanced diagnostics, surgery, advanced medicines, and tissue and bone replacements.

Since the discovery of carbon nanotubes,[6] one-dimensional (1D) nanostructures have become an important focus of research in nanoscience and nanotechnology. These nanostructures enable unique quantum effects that directly impact the electronic and optical properties. Therefore, they are showing great potential both in understanding size-dependent electrical, optical, thermal and mechanical properties and in fabricating nanosized electrical junctions, optoelectronic and electromechanical devices.[7] At the same time, the fundamental interests come from the nanometer scale that bridges the microscopic world where the behavior of matter needs to be treated in quantum mechanics and the macroscopic world where quantum mechanics reduces to classical physics. Studies on the preparation, structure, and properties of nanostructures have been carried out with collective efforts that cross borders between many areas of physical sciences, engineering and biological sciences.[8] Furthermore, unique or enhanced properties have also been revealed from these nanostructures due to their high surface-to-volume ratio, size confinement effect, and high-quality crystallinity. As a result, nanostructures are found to possess unique or enhanced properties compared with their bulk counterparts and more and more devices continue to utilize these properties.[9] Numerous novel applications have thus been proposed and even demonstrated in laboratories in diverse fields of optics, electronics, mechanics, and biomedical science. Recently, more and more interest in nanostructures has been driven by not only

fundamental sciences but also their potential applications.

The term “nanowire”, which represents any wire-like structure with a diameter less than 100 nanometers, is widely used to represent one-dimensional nanostructures. Not only the size variation, composition and shape alteration of nanowires are also result in changes of optical, electronics, magnetic, mechanical and chemical properties of materials.[10, 11] Nanowires, which have been the subject of intense research activity in recent years,[8] have been studied intensively not only because low dimensionality and their interesting intrinsic properties, but also due to their unique properties arising from quantum confinement effects and their capability for direct nanosystem integration.

As inspired by their unique characteristics, nanowires, such as semiconductor[12] and metal oxide nanowires,[8] have become the research forefront in nanoscience and nanotechnology. Recently, more and more nanowires have been drastically developed from different materials by various kinds of methods, and these nanowires have been found to possess excellent mechanical, electrical, optical and thermal properties compared with their bulk states. These nanowires are therefore expected to be key elements of future technologies and will be widely used to overcome worldwide issues in energy, food, health, etc. Needless to say, in many cases for particular applications, further research and development are needed to resolve the wide gap that exists between research status and their availability for practical applications.

The composition of nanowires can be single crystal, poly-crystal, amorphous or

organic chains. The ideal materials for many applications should be single-crystalline and defect-free, and single-crystalline nanowires are the most intensively studied structure owing to their unique electronic, optical, mechanical and magnetic properties.[8, 14] A single-crystal nanowire grows along a specific axial direction, whereas their side surfaces may or may not be well-defined. The cross-section of a nanowire can be round, hexagonal or polyhedron according to the crystallography of the material. The length of a nanowire varies from a few hundred nanometers to microns or even millimeters. However, its thickness is always negligibly small comparing to its length. Sometimes, the terminology nanorod is also applied to describe a short nanowire with lengths ranging from tens to hundreds of nanometers.

Recently, semiconductor nanowires, which are considered to be the critical components in a wide range of potential applications of nanoscale devices, have become the focus of intensive research. They possess novel properties intrinsically associated with low dimensionality and size confinement.[14, 15, 16]

More recently, the steadily growing interest in Cu_2O nanowires can be attributed to several reasons. First, Cu_2O is one of the first known non-stoichiometric p-type semiconductors with a direct band gap of ~2.17 eV,[17] which makes it a potential photovoltaic material in solar cells.[17, 18, 19, 20, 21] An enhancement in photocurrent for dendritic branched n-type Cu_2O has also been reported recently.[22] Second, Cu_2O nanostructures have shown their promising applications in many fields, such as high

performance gas sensor[23, 24] catalysis,[25, 26] negative electrode materials for lithium ion batteries,[27] and photo activated splitting of water under visible light irradiation.[28] In addition, compared with the commonly used semiconductors, such as Si and GaAs, Cu_2O is low-cost, non-toxic, good environmental acceptability, and can be prepared in large quantities because of natural abundance of copper.

During the last couple of years, inspired by the realization of their applications in different fields, various methods have been developed to fabricate Cu_2O nanowires. The essence of nanowire formation is crystallization, a process that has been investigated for hundreds of years. The evolution of a solid from a vapor, liquid or solid phase involves two fundamental steps: nucleation and growth. With a continuous supply of the materials, these nuclei serve as seeds for further growth to form a long-range-ordered, crystalline lattice. In addition, the building blocks also need to be supplied at a well-controlled rate in order to obtain crystals with a homogeneous composition and uniform morphology. The most common approach is the template-based electrochemical deposition in a copper lactate solution, in which the Cu_2O nanowires are formed in porous templates, such as anodic aluminum oxide or track-etched polycarbonate.[29, 30, 31, 32, 33] Template-based synthesis is a convenient method for generating nanostructures. In this technique, various porous structures are used, and nanomaterials can be synthesized within the pores. This technique involves the electrochemical deposition, either electrolytic or electroless, of a material onto a membrane structure containing randomly, or regularly dispersed, uniform

nanopores. Although electrodeposition into nanoporous templates is an attractive method for producing aligned nanowire arrays with uniform and controllable dimensions, this technique leads to complicated processes and also needs to remove template to obtain the individual nanowires. The technique is suboptimal for production of single crystals providing high charge-carrier mobility. Moreover, the yield is relatively low. Other methods require solution-based chemical synthesis, involving the reduction of a copper sulfate in the presence of a suitable surfactant.[34, 35, 36, 37, 38, 39] Such techniques for growing Cu_2O nanowires, however, have required the use of catalysts, or other starting materials. They are often based on special instruments or harsh conditions, and it is hard to control the whole fabricating process. Moreover, Cu_2O and CuO nanowires have also been fabricated from the thermal oxidation of Cu_2S nanowires under oxygen at and above 300°C.[40] But Cu_2O and CuO nanowires fabricated from the method are poly-crystalline ones.

In a word, on the basis of the aforementioned approaches, the fabrication of Cu_2O nanowires demands special conditions, complex process control, expensive chemicals, time-consuming and so on. Furthermore, Cu_2O nanowires fabricated by the aforementioned methods are sometimes not sufficiently good enough traits due to a low degree of material crystallinity, and their low aspect ratio makes device fabrication and further potential applications difficult.[31, 32, 36]

On the other hand, growth of dense CuO nanowires has been generated on copper substrates including grids, foils and wires when these substrates were heated in air or oxygen environment at 400-700°C.[41, 42, 43, 44, 45, 46] This approach is named stress-induced method or thermal oxidation method. The most likely explanation for the stress-induced method is based on the effects of compressive stress, which results from the different thermal expansion coefficients, on the formation of nanowires. The mechanism may be easily understood by considering a simple phenomenon in a street where people migrate from a crowded area to an uncrowded area.

In addition to the above mentioned, other nanowires or nanowhiskers fabricated by this stress-induced method have been studied extensively, such as Sn nanowiskers,[47] Si nanowires,[48] Cu nanowhiskers,[49] Bi nanowires,[50, 51], and Al nanorods[52] etc. A mechanism for the spontaneous growth of Sn nanowhiskers was proposed by researchers.[47] The driving force for evolution of Sn nanowhiskers is a biaxial compressive stress developed in Sn deposits by the formation of an intermetallic compound of Cu_6Sn_5, especially in grain boundaries of Sn films. The biaxial compressive stress gives rise to strains normal to the film plane, which are dependent on the Sn grain orientations. The stress-driven formation of Si nanowires was presented by other researchers.[48] The Si nanowires grew directly from the silicon substrate, they do not need to be manipulated or aligned for subsequent applications. In this research, the critical parameters in the growth of these nanowires are the surface treatment and the carrier gas used. Some researchers reported

the rapid and mass growth of Cu nanowhiskers on polycrystalline films.[49] The diameters and lengths of the nanowhiskers are governed by temperature, film thickness, grain size and time. Cu atoms diffuse due to local stress gradient in the grains which originate in the material singularities and geometrical singularities caused at the grain boundaries by anisotropy of the grains. Weak spots in the oxide layers on the films act as initiation sites for the nanowhiskers. Other researchers reported to make Bi nanowires by this method.[50] These nanowires were extruded spontaneously at the rate of a few micrometers per second at room temperature from the surfaces of freshly grown composite thin films consisting of Bi and chrome-nitride. The high compressive stress in these composite thin films is the driving force responsible for the nanowire formation. Some researchers reported that single crystalline Bi nanowires were found to grow on as-sputtered films after thermal annealing process.[51] This was facilitated by relaxation of stress between the film and the thermally oxidized Si substrate that originated from a mismatch of the thermal expansion. Other researchers reported Al whiskers grown on aluminum thin films during heat treatments, and investigated the influence of the aluminum film properties and the conditions of the heat treatment on whisker nucleation and growth.[52] Their results indicated that breaking Al surface oxide and/or atom rearrangement through surface diffusion has a critical role in the growth process of whisker.

Compared with other methods for fabricating nanowires, this stress-induced method is quite simple and efficient, and here for copper oxide nanowires only metallic Cu and Ta

powder and silicon substrate are used, without any catalyst, additive, complex procedure, or buffer layer. This method is low cost without any chemical reaction. It takes the advantage of simple procedure and high-yield performance. Moreover, the as-obtained nanowires are of orderly distribution, high-quality and fine crystal structures such as bicrystal[41] and single crystal.[46, 51,52] Heating temperature is reported to be a key factor to control diameters of the as-obtained nanowires.[41, 44, 49]

However, for copper oxide nanowires, nanowires fabricated at such a high temperature are CuO nanowires rather than Cu_2O ones. Recently, the above-mentioned growth of nanowhiskers from Cu thin films deposited on SiO_2/Si substrate at a heating temperature of 340°C had been realized,[49] where the products were mentioned to be Cu nanowhiskers without detailed investigations of their morphology and microstructures.

In the dissertation research, the simple and efficient stress-induced method would be explored to fabricate high-quality Cu_2O nanowires free from drawbacks of other fabrication methods. Once come true, it would become a significant breakthrough in the domain of nanowire fabrication.

1.2 Current Research Challenges

To date no simple method has been found for fabricating Cu_2O nanowires over large areas with fine structures. Therefore, developing a novel strategy, which allows one to easily grow the desired Cu_2O nanowires with high-quality crystallinity and high aspect

ratio in a simple manner, can provide valuable tool to explore their unique properties.

Moreover, there are few reports on the study of controllable Cu_2O nanowires which are required by the continued development of Cu_2O nanowire-based nanodevices. Until now, the ability to tightly control the physical properties of the Cu_2O nanowires including diameter and aspect ratio remains a significant challenge. In addition, the mechanism for nanowire growth under this stress-induced method is still not well understood, and research on growth mechanism would lead to fundamental understanding of this method.

It would be highly beneficial if the technique of desired nanowire growth at predetermined positions can be combined with traditional silicon microfabrication technologies in the pursuit of next-generation high-performance nanodevices.

Another challenge is to open up more potential applications in more fields.

1.3 Research Goal and Objectives

The main objective of this work is the fabrication of uniform copper oxide nanowires.

The research objectives of this dissertation are therefore to:

Project Goal #1: Fabrication of uniform and high-quality nanowires. The stress-induced method would be used to fabricate copper oxide nanowires. Effect of various parameters would be investigated as to how they affect the nanowire growth. The aspect ratio, diameter and composition of nanowire and geometry would be investigated. Finally, the optimum growth condition would be found.

Project Goal #2: Control of nanowire diameter. It is important to work out a simple and accessible way to control nanowire diameter for future applications.

Project Goal #3: Analysis of growth mechanism. By understanding the mechanism behind the nanowire growth, the ultimate goal is to control with atomic precision morphology, structure, composition, and size of nanoscale materials, so as to enable precise control over the properties of the resulting nanowires.

Project Goal #4: Nanowire growth at predetermined positions with desired patterns. This research may set bedrock for scale-up, mass production, and many industrial and commercial applications for the future of nanotechnology.

Project Goal # 5: Application for their photovoltaic effect. Further experimental and theoretical research on copper oxide nanowires for solar cell can explore a brand new way to produce high-efficient and low-cost photovoltaic devices.

1.4 Outline of the Dissertation

As an active field in nanotechnology, a systematic study on the fabrication and application of copper oxide nanowires is presented in this dissertation. In particular, copper oxide, one of the most important functional semiconducting materials with optical and magnetic properties, is the core objective of this research, from nanowire fabrication, the controllable diameter of nanowires to understanding their growth mechanism, nanowire growth at predetermined positions, and to how to expand their applications.

This research may set a foundation for many industrial applications from controlled fabrication to nanomanufacturing.

The main text of this dissertation is organized into six chapters, as follow:

Chapter 1 describes research background and motivation, current research challenge, and research goal and objective in this dissertation.

Chapter 2 gives the detailed fabrication process of nanowires and how to evaluate these nanowires. The experimental procedure, which investigates the effect of cooling process on nanowire growth, namely direct cooling and gradual cooling process, is given in detail. In particular, the procedure for figuring out the optimum growth condition for nanowires is presented in the chapter. For control of nanowire diameter, adjusting the thickness of the deposited Cu film is proposed to fabricate copper oxide nanowires with different diameters. Moreover, the component and characterization of as-obtained nanowires are also analyzed using Scanning Electron Microscopy (SEM), X-ray Diffraction (XRD), Energy Dispersive X-ray Spectroscopy (EDXS), Transmission Electron Microscopy (TEM) and High Resolution Transmission Electron Microscopy (HRTEM) in the chapter. It arrives at a crucial conclusion that the component of these as-obtained nanowires is Cu_2O rather than CuO.

Chapter 3 details the analysis of nanowire growth mechanism in this research. A detailed discussion is given about the stresses in the copper film, heating process and cooling process.

Chapter 4 presents nanowire growth at predetermined positions with desired patterns. The fabrication process for this part is demonstrated step-by-step.

Chapter 5 elaborates photovoltaic application, in which the sample with Cu_2O/Cu junction is prepared, and dark current curve and photovoltaic current density-voltage curve are measured.

Finally, summary of the most important conclusions and the future work in the dissertation research is presented in chapter 6.

Chapter 2 Fabrication and Evaluation

One-dimensional nanostructures, such as nanowires and nanotubes, demonstrate their anisotropic properties which have been realized in various applications including electronics, optics, catalysis, and biomedicine. The synthesis of nanowires is one of the most active fields in nanotechnology. Fabrications of nanowires are drastically developed during the past decade.[13] Fabrication methods can be divided roughly into two groups: top-down and bottom-up methods.[53] They are two distinct concepts for realizing structures and devices in nanometer scale. Top-down methods start with patterns made on a large scale and reduce its lateral dimensions before forming nanostructures. On the other hand, bottom-up methods begin with atoms or molecules to build up nanostructures, in some cases through smart use of self-organization.

Top-down methods start from bulk materials, which are sculpted into nanosized features by carving, milling, etching and patterning. Electron beam-, photo-, nanoimprinted-, and scanning probe-lithography are considered powerful top-down methods for nanowires synthesis. Template-based methods are typical examples of this method. By using a nanopore array as a template, nanowires can be created within a confined volume and space limited by the pores structures, then the template can be etched or removed leaving the desired nanowires behind. The nanowires made by this method can be produced in a wide range of materials. A number of templates, such as

nanoporous membranes, surfactants, and biomolecules, have been successfully exploited for nanowire fabrications. Types of templates include hard template, soft template, and biomolecular template. It is noticed that top-down methods are the time-consuming protocols and don't fabricate a free-standing nanowire. Moreover, the techniques are not practical for mass fabrication of nanowires as compared to the "bottom-up" method discussed below.

Bottom-up method is a construction of the nanowires using atomic building blocks. Underpinning this bottom-up paradigm is the controlled growth of nanoscale materials, the fundamental building blocks, pursued within the disciplines of materials science and chemistry. In such methods, the atoms and molecules are assembled into the smallest nanostructures (dimension of typically 2 to 10 nm) by carefully controlled chemical reactions, which make this technique cheaper as compared to the above discussed top-down methods. Self-assembly of atoms and molecules into nanostructures can be classified as a bottom-up method. In nature self-assembly is often used to make complex structures, which holds great promise in nanostructures. This level has been the most active area in nanotechnology and a large variety of morphologies has been discovered or created. Up to now, many methods belong to bottom-up method have been developed to fabricate nanostructures, and they have been classified in two categories: self-patterning via physical routes and self-patterning via chemical routes.[54] The first one employs well-known physical growth concepts, such as island growth. It is based on the

phenomenon that the initial growth of an epitaxial film deposited on the single-crystal substrate with high lattice mismatch, would result in island or layer-then-island growth mode. Those two growth modes are suitable to grow crystalline nanosize (quantum) dots. The latter method uses simple chemical routes (for instance, the microemulsion concept) to fabricate nanosize crystals or nanoparticles in colloidal suspensions, which can be later spread onto the substrate. After solvent evaporation, the nanoparticles can be crystallized in two- or even three-dimensional arrays. The bottom-up methods mainly use naturally formed and rather well-defined structures. The method is possible to form nanowires at lower costs and on a larger scale as compared to the top-down method, which is the greatest advantage.

In recent years, single-crystal Cu_2O nanowire arrays have attracted research interest because they may be used as building blocks for a new generation of devices in different technological domains. Its broad application prospect has triggered focused research in the development of numerous growth methods with low-cost and accessibility to synthesize Cu_2O nanowires over the past decade. Nevertheless, many challenges of fabricating Cu_2O nanowires, such as exploring simple, cheap, catalyst-free methods and so on, still remain.

Of these method, the stress-induced method, which is a common example of the bottom-up approach, is normally the first choice as it is simple to setup and gives acceptable control of the process. The fabrication process based on this method has been

employed for fabricating Cu_2O nanowires with single crystal and high aspect ratio, which composes the core of this dissertation. Therefore, the discussion of the research starts with this chapter, which covers the details of experimental procedure and setup, direct cooling process and gradual cooling process, the optimum growth condition, control of nanowire diameter, and component of as-obtained nanowires.

2.1 Experimental Procedure

The first step in the procedure is to prepare the multi-layer sample. A Tantalum (Ta) layer of 60 nm in thickness was deposited on a 0.28 mm thick Si [100] substrate covered with a 300 nm thick SiO_2 layer by the electron beam evaporation (EBE) technique. In order to create uniform and high-quality thin film in the case, the deposition rate of the thin film was kept constant. Tantalum has exhibited excellent diffusion barrier effects against Cu superior to Ti, Cr, Nb and Mo, and has been considered as a most favorable diffusion barrier for Cu.[55, 56] Moreover, Ta demonstrates enhanced Cu texture and strengthened adhesion between the SiO_2 layer and the subsequently deposited Cu layer. Hence, Ta is one of the most promising under-layer materials for Cu-based materials. A Cu film was then deposited on the Ta layer by the same technique to form the $Cu/Ta/SiO_2/Si$ system as shown in Figure 2.1. The thickness of the Cu films was controlled by the deposition time, and the typical thickness of the Cu layer is around 400 nm in the experiment. As the sample was placed in the atmosphere, the surface of the Cu layer was naturally oxidized

and covered with a thin layer of Cu_2O.[57]

Figure 2.1 Schematic multi-layer sample.

The experiment was conducted under atmospheric conditions, and a ceramic heater positioned beneath the sample heated the samples uniformly in order to produce thermal compressive stress in the Cu layer which is needed for stress-induced growth of nanowires. When the Cu/Ta/SiO_2/Si system was fabricated at room temperature, there was almost no stress in all the layers. The compressive stress appeared in the Cu films immediately after starting the heating. The temperature was kept constant monitored by a thermocouple. By controlling the voltage of the power supply, the heating temperature can be adjusted to the required value. During the heating process, the Cu layer endured a compression applied on its bottom face due to the mismatch of thermal expansion in different layers. To keep the deformation compatibility of the whole system, circumferential tension or compression stresses occurred in all the layers due to their different thermal expansion coefficients. The Cu film expanded when it was annealed at

340°C, while the SiO_2/ Si substrate restricted the expansion, putting the Cu film under compressive stress. The hydrostatic stress was found to be uniform on a macroscopic level all over the Cu thin layer. The Cu atoms migrated towards the top surface of the Cu layer due to the stress gradient and penetrated the oxide layer via any weak spots to form nanowires. Therefore, the spontaneous growth of the nanowires becomes a means of relieving the compressive stress.

After heating for different times at 340°C, the samples were cooling either directly or gradually for different times respectively to investigate the effects of cooling procedure on nanowire growth. In the gradual cooling process, the voltage of the power supply was decreased step by step to produce the gradually reduced temperature during a certain period.

The samples with nanowire arrays were observed by different kinds of special equipment. The morphology and structure of nanowires were characterized using a field emission scanning electron microscope (FE-SEM). The further microstructure and composition of samples was examined by transmission electron microscopy (TEM), selected-area electron diffraction (SAED), and the high resolution transmission electron microscopy (HRTEM)). The composition of the nanowires was also analyzed by energy dispersive X-ray spectroscopy (EDXS) and X-ray diffraction (XRD).

To prepare TEM samples, nanowires were dispersed in alcohol by sonication for 2 min. A small drop of the solution containing the nanowires was dropped on a Cu grid covered

with carbon film and dried in air. To obtain more accurate results, oxidation of the nanowires must be avoided. Therefore, the entire sample preparation procedure was carefully carried out. The TEM grid with nanowires on it was put into vacuum chamber, and the sample was observed by TEM as soon as possible.

2.2 Direct Cooling Process and Gradual Cooling Process

After being heated for 3~9 hours at 340°C, the samples were cooled either directly or gradually for 2, 3, 4 ,5 or 7 hours respectively to investigate the effects of cooling process on nanowire growth.

The sample cooled directly is observed to be covered with dense nanowires, as shown in Figure 2.2 a. Figure 2.2 b shows the side view of nanowires growing on the substrate. As seen in the side views, all nanowires are almost vertically aligned. The average length of these nanowires is approximately 2 μm and their growth density, the number of nanowires per unit area, is about $10^9/cm^2$.

For the samples undergone the gradual cooling process, some randomly distributed hillocks on the multi-layer substrate with much longer and denser nanowires than those growing on the substrate, are observed, as shown in Figure 2.3 a-c.

This phenomenon does not appear for samples under direct cooling process, which indicates that the hillocks and nanowires on them can be generated during the gradual

cooling process, even though these samples have been heated for 9 hours and cooled directly.

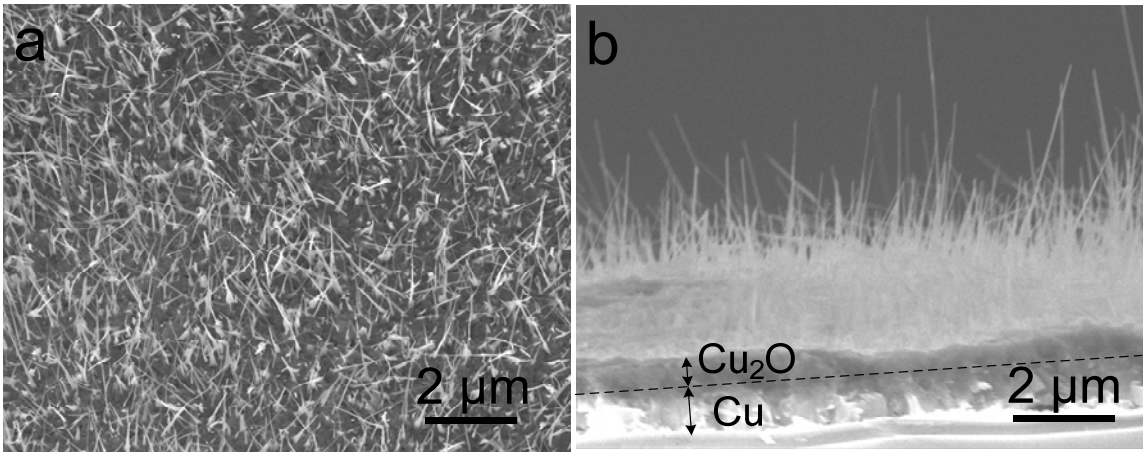

Figure 2.2 SEM images of nanowires fabricated after heating under direct cooling process. (a) nanowires growing on the substrate, (b) the side view of nanowires growing on the substrate.

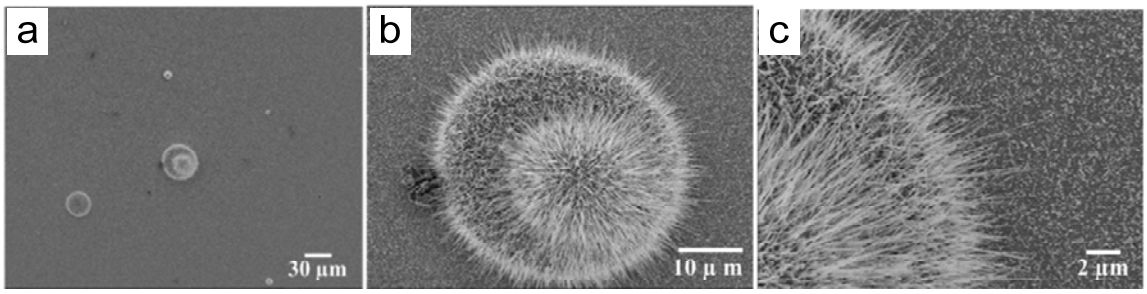

Figure 2.3 SEM images of nanowires fabricated after heating under gradual cooling process. (a) hillocks on the substrate, (b) hillocks of low-magnification view, (c) hillocks of high-magnification view.

This phenomenon has not been reported elsewhere that the nanowire growth is affected

by cooling process by the stress-induces method. Therefore, it provides a positive view for the fabrication of nanowires with much higher aspect ratio by introducing the gradual cooling process.

2.3 Optimum Growth Condition

In this part, systematic study on the nanowire growth conditions is focus on. This study aims at determining the optimum growth condition for nanowires.

Here, a series of experiments for different heating and gradual cooling times, as shown in Table 2.1.

Table 2.1

Heating time / Cooling time	**3 h**	**4 h**	**5 h**	**6 h**	**9 h**
2 h			10-50 nm /0.4-7.6 μm Sparse		
3 h	5-40 nm/ 0.3-0.9μm Moderate	5-50 nm /0.4-8μm Moderate	10-50 nm /0.8-10.3 μm Moderate	10-55 nm/ 0.6-10.3μm Moderate	
4 h	5-45 nm /0.4-1.3μm Moderate	5-40 nm /0.3-2 μm Moderate	10-50 nm /1.3-14.7 μm **High density**	5-55 nm/ 0.3-10.8 μm Moderate	10-50 nm /1.1-2.6μm Moderate
5 h	5-40 nm /0.3-0.8 μm Sparse	5-55 m/ 0.5-12 μm Moderate	5-45 nm /0.2-6.1 μm Sparse	5-55 nm /0.3-12 μm Moderate	
7 h	3-40 nm /0.2-0.6 μm Sparse		5-45 nm /0.2-1.1μm Sparse		

Nine typical SEM images of nanowire growth for different heating and gradual cooling times are presented in Figure 2.4.

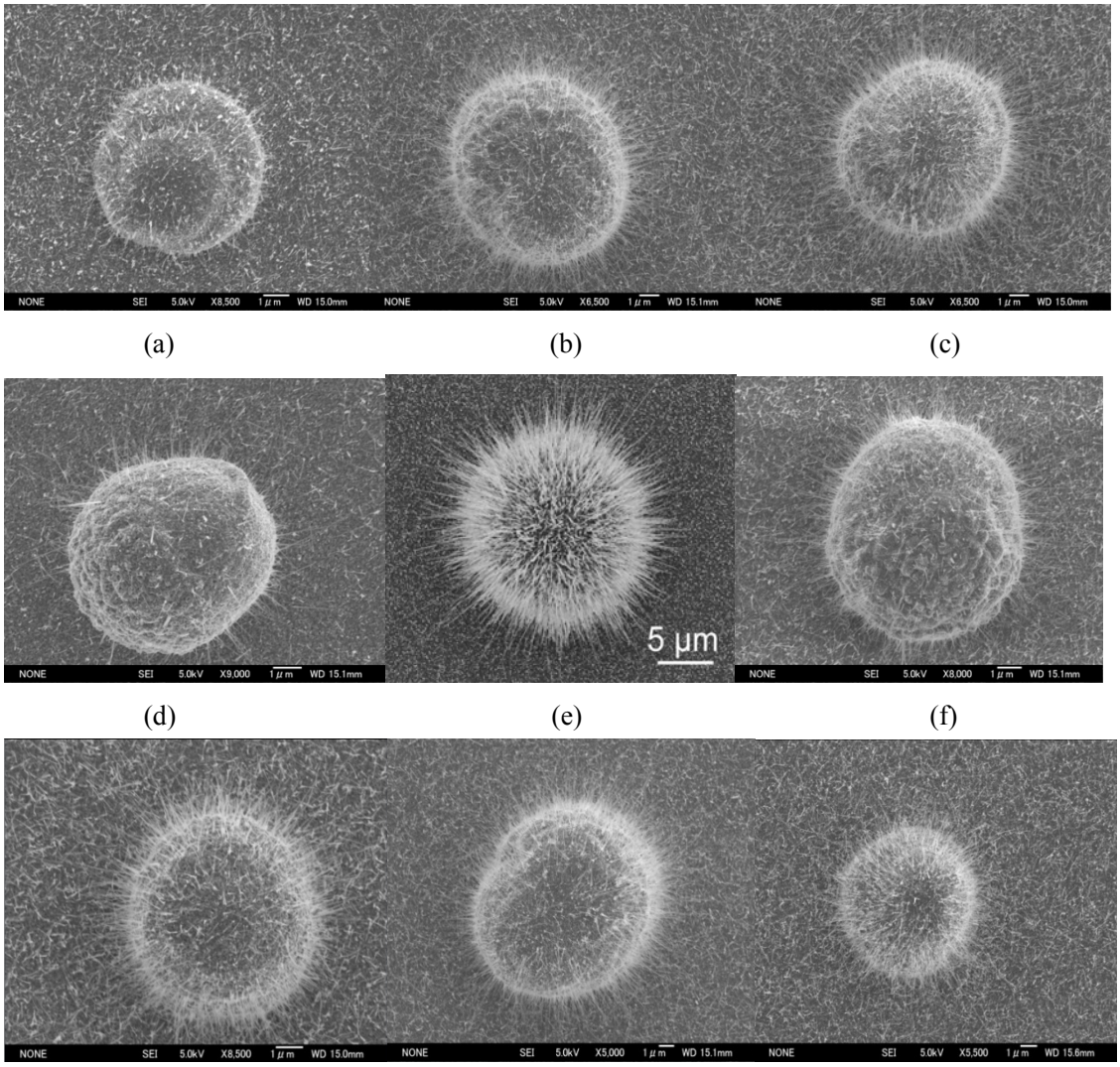

(a) (b) (c)

(d) (e) (f)

(g) (h) (i)

Figure 2.4 SEM images of nanowire growth for different heating and gradual cooling times. (a) Heating 4 h and cooling gradually for 3 h, (b) Heating 5 h and cooling gradually for 3 h, (c) Heating 6 h and cooling gradually for 3 h, (d) Heating 4 h and cooling gradually for 4 h, (e) Heating 5 h and cooling for gradually 4 h, (f) Heating 6 h

and cooling gradually for 4 h, (g) Heating 4 h and cooling gradually for 5 h, (h) Heating 5 h and cooling gradually for 5 h, (i) Heating 6 h and cooling gradually for 5 h.

From these results, it is very obvious to find the optimum growth condition: the heating continues 5 hours at 340℃, then cooling gradually the sample over 4 hours.

The temperature profiles during the 5-hour-heating and cooling (either directly or gradually for 4 hours) process are shown in Figure 2.5 (a) and (b). The cooling rate during the 4-hour-cooling process is 1.31°C/min.

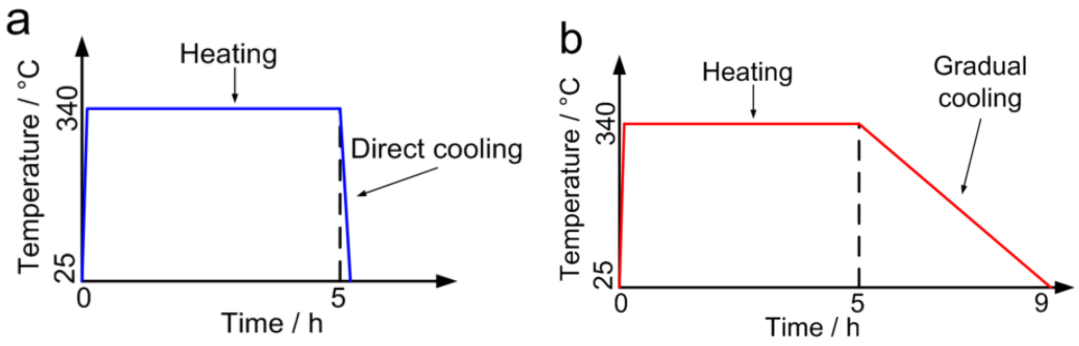

Figure 2.5 Temperature profiles of (a) heating and direct cooling process, and (b) heating and gradual cooling process.

SEM images of nanowire growth under the optimum growth condition are shown in Figure 2.6.

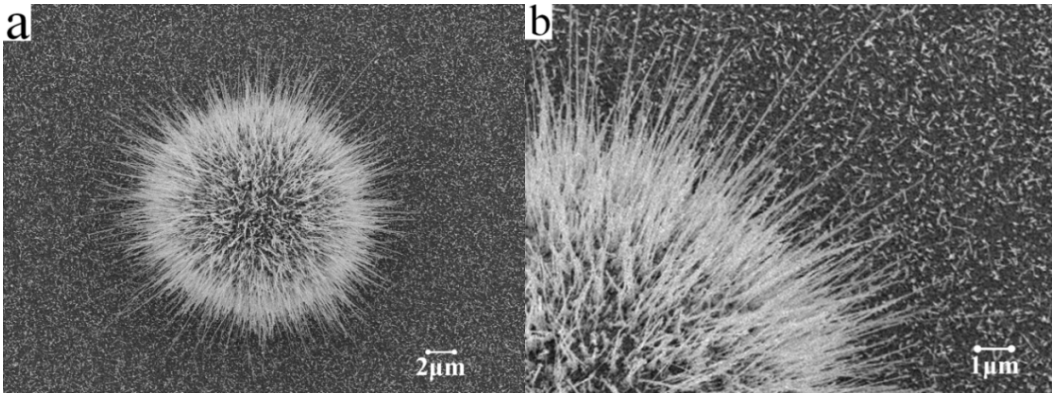

Figure 2.6 SEM images of nanowires growing on hillocks under the optimum growth condition. (a) 3000 times, (b) 7500 times.

FE-SEM analysis shows that nanowires growing on the hillocks in the main range of 10-50 nm in diameter can reach up to 15 μm long, nearly seven times longer than those growing on the substrate and those reported in reference.[47] The largest aspect ratio is not less than 300 and the growth density is even higher than $10^9/cm^2$.

In this part, different heating times have been tried to study their effect on the length of the nanowires. As shown in Figure 2.7, heating for more than 5 hours leads to the similar length of the nanowires, which is about 2 μm in average.

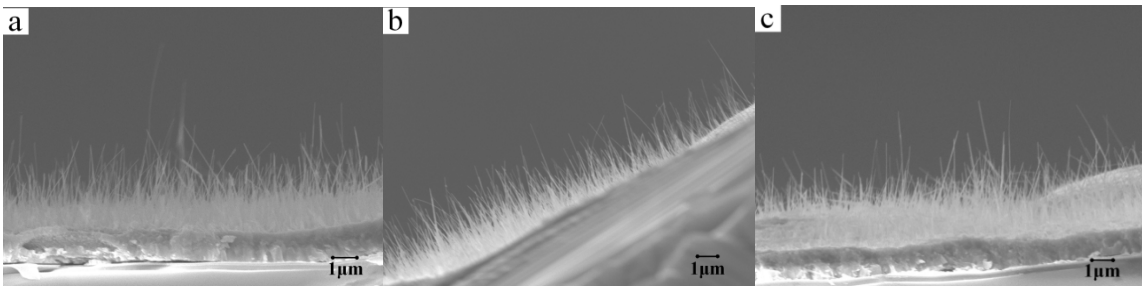

Figure 2.7 SEM images of the nanowires growing on the substrate after heating for (a) 5, (b) 6, and (c) 7 hours.

Herein, the effect of the cooling process on nanowire growth is demonstrated to be a key factor for obtaining nanowires with larger aspect ratios and for further improving the growth density of nanowires. The optimum growth condition of heating for 5 hours and gradual cooling for 4 hours is proposed for the first time.[58] Although some researchers also investigated the effect of cooling time on the growth of Bi nanorods,[59] they only arrived at conclusion that the nucleation and growth of Bi nanorods might take place during the cooling time by observing growth morphology and growth trends.

In summary, the mass production of nanowires by the stress-induced method has been achieved, and better quality nanowires with higher density and larger aspect ratio are obtained. The optimum growth condition is put forward, with the emphasis on the effect of cooling process on nanowire growth in the part.

2.4 Control of Nanowire Diameter

Nanotechnology represents one of the exciting frontiers in modern science and engineering research. Fabricating desired nanowires in a well-controlled way represents one of the most difficult challenges facing today's researchers and engineers in nanotechnology research. Structure, morphology, and dimensionality control of nanowires during fabricating process is essential and can strongly encourage the further development for much more practical applications.

High-quality copper oxide nanowires with controllable diameter are really needed. The

morphology structure of nanowires can greatly influence their properties, which further affects their final applications. High-quality copper oxide nanowires can also induce enhanced properties and novel applications.

Many researchers have investigated controllable size of other material one-dimensional nanostructures,[51, 60, 61, 62, 63] such as silicon nanowires, carbon nanotubes.

So far, there are few reports on the study of controllable copper oxide nanowires which are required by the continued development of copper oxide nanowire-based nanodevices. The ability to tightly control the physical properties of the copper oxide nanowires including diameter and aspect ratio remains a significant challenge until now. It is urgent to find a cost-effective and simple way to control nanowire diameter.

Since the nanowire growth by the stress-induced method is closely related to the microstructures of the grains and grain boundaries on the surface of the samples, it can be deduced that the grain size may have some relation to the nanowire diameter. In this part, the study on the relation between the thickness of the Cu film and nanowire diameter has been investigated in detail.

In order to study the influence of thickness of Cu films on the nanowire diameter, samples with different thicknesses (200, 400, 600 and 800 nm) of Cu films were prepared by controlling the EB evaporation time at the same deposition rate.

Samples with different thicknesses of 200, 400, 600 and 800 nm of Cu films were heated under the optimum growth condition, and then were investigated by SEM. The

micrographs of nanowires growing on hillocks and substrates are shown in Figure 2.8 and Figure 2.9, respectively. It can be observed from the two figures that the growth of nanowires with smaller (larger) diameter is favored in the presence of thinner (thicker) Cu films. The results reveal that nanowire diameter is strongly dependent on the thickness of the Cu film.

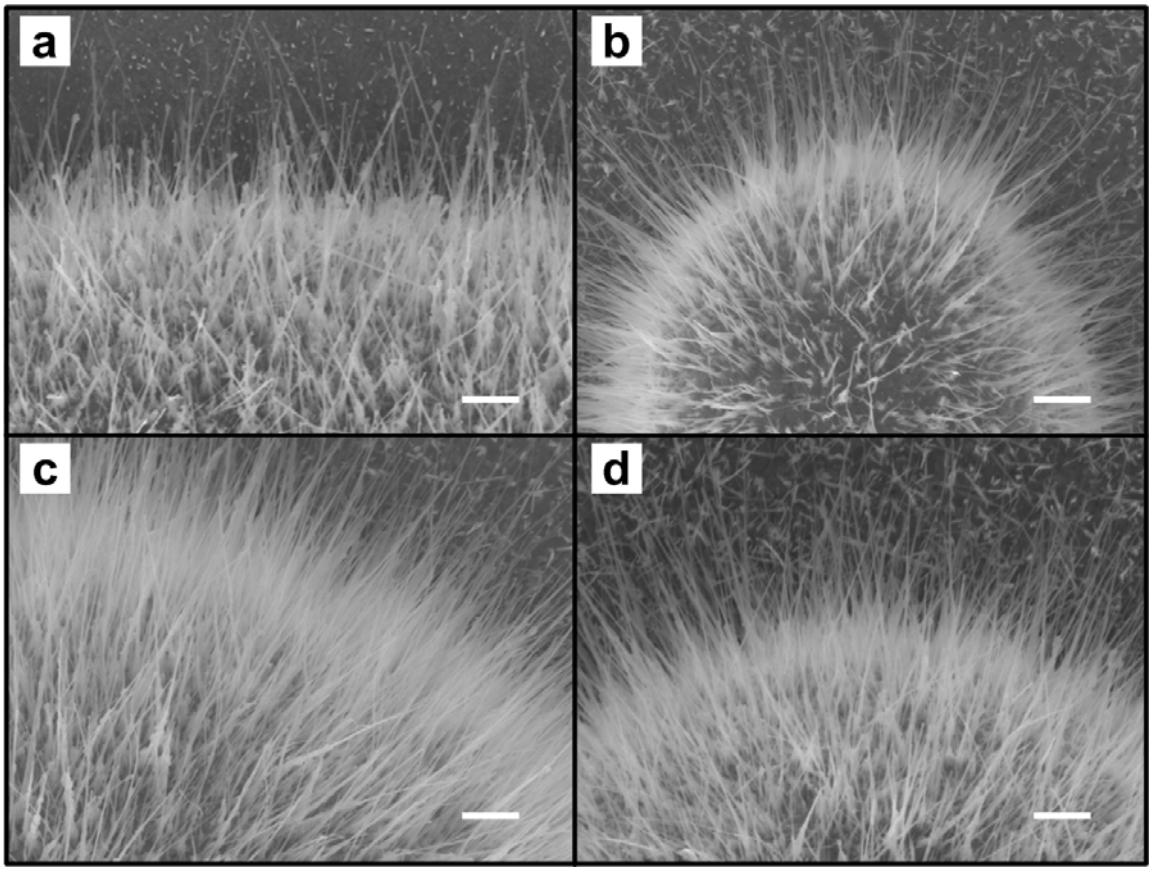

Figure 2.8 Micrographs of nanowires growing on hillocks of Cu films with different thicknesses of (a) 200, (b) 400, (c) 600, and (d) 800 nm. The scale bar is 1μm.

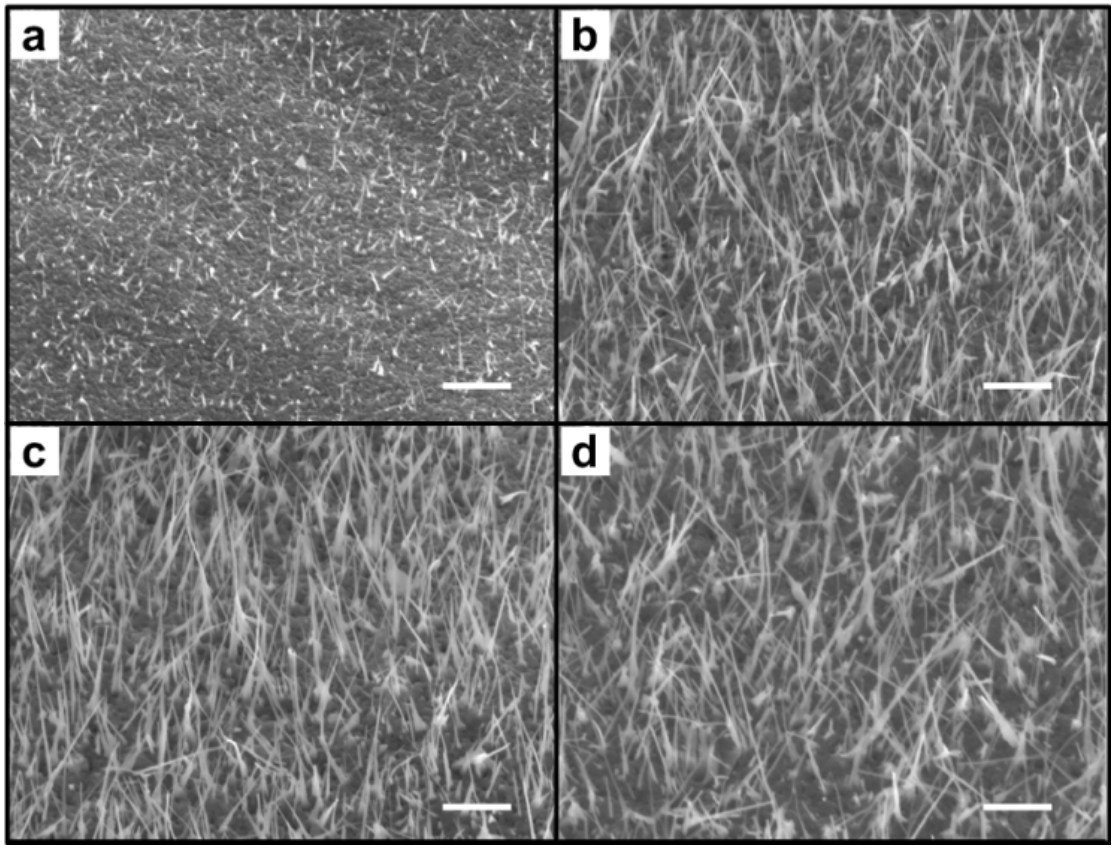

Figure 2.9 Micrographs of nanowires growing on the substrates of Cu films with different thicknesses of (a) 200, (b) 400, (c) 600, and (d) 800 nm. The scale bar is 1 μm.

To quantify the diameter distributions of nanowires growing on the hillocks which have been generated from Cu films with different thicknesses, an extensive SEM analysis is carried out. Histograms of the nanowire diameters corresponding to Cu films with different thicknesses are plotted in Figure 2.10. For nanowires growing on hillocks which are generated from 200, 400, 600 and 800 nm thick Cu films, the average diameters are calculated from the statistical results over 100 nanowires to be 24.3, 31.3, 42.1, and 51.3 nm, respectively. Detailed descriptions of the statistical results are as follows. For Cu film

thickness of 200 nm, it is possible to determine the nanowire diameter in the range of 20-30 nm with a distribution percentage of approximately 43%. For Cu film thickness of 400 nm, it is possible to determine the nanowire diameter in the range of 30-40 nm with a distribution percentage of approximately 54%. For Cu film thickness of 600 nm, it is possible to determine the nanowire diameter in the range of 40-50 nm with a distribution percentage of approximately 50%. For Cu film thickness of 800 nm, it is possible to determine the nanowire diameter in the range of 50-60 nm with a distribution percentage of approximately 53%. Histograms of the nanowire diameters obtained from SEM analysis demonstrate a close correlation between nanowire diameter and the thickness of Cu films. In addition to the close correlation between nanowire diameter and the thickness of Cu films, it is also found that the diameter dispersions of nanowires corresponding to Cu films with different thicknesses are similar. Almost more than 80% of the nanowires growing from the same sample have their diameters in a narrow range of ±15 nm with respect to their average diameter.

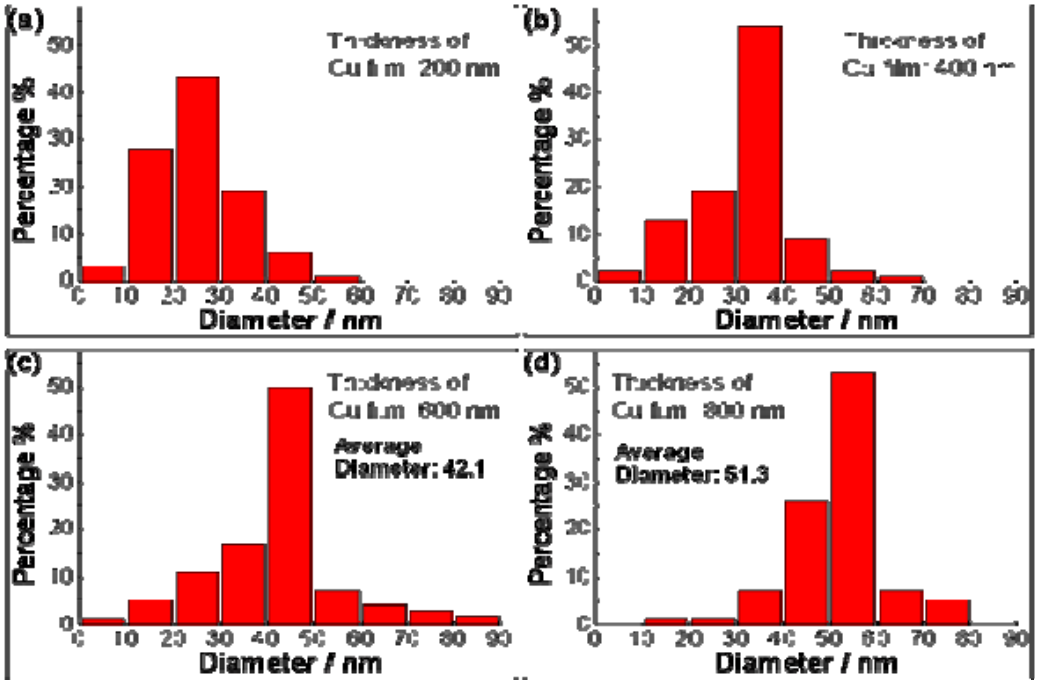

Figure 2.10 Histograms of diameter of nanowires growing on different Cu film thicknesses.

A brief interpretation for the influence of Cu film thickness on nanowire diameter is given as follows. Before the thermal treatment, the mean grain sizes for Cu films with different thicknesses of 200, 400, 600, and 800 nm are observed to be 21.3 nm, 27.3 nm, 35 nm, and 41.9 nm, respectively. The mean grain size and the average diameter of nanowires are plotted as functions of Cu film thickness in Figure 2.11. These results demonstrate that the nanowire diameters depend on the mean grain sizes of the Cu films, which are determined by the thickness of the Cu films. Since the grains on the surface of the Cu films offer the initial nucleation sites for the nanowire growth, it is reasonable that the mean grain size is critical to determine the diameter of the nanowires. Thus, thicker

Cu films with larger mean grain sizes can give rise to nanowires with larger diameters. In addition, thermal compressive stress in the Cu film during the heating process drives the migration of Cu atoms from the interior to the surface of the Cu film, and plays an important role in nanowire growth. In thinner film, the migration of Cu atoms from the interior is less. Therefore, the available number of Cu atoms is also very less. Hence the growth rate is low, which results in the smaller nanowire diameter. As the thicknesses of Cu films are increased, a large number of Cu atoms can cross the metal/metal oxide interface to form nanowires. In other words, the migration of Cu atoms in a thicker Cu film from the interior to the surface of the film is more plentiful than that in a thinner Cu film. Therefore, plenty of available Cu atoms on the film surface can react continuously with surface absorbed oxygen, leading to formation of nanowires with larger diameters.

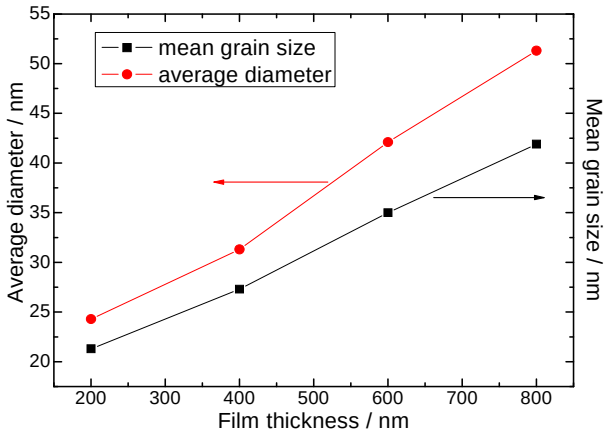

Figure 2.11 Mean grain size of Cu film and the average diameter of nanowires varying with Cu film thickness.

The influence of film thickness on the length of nanowires is also investigated, but no obvious dependence between them can be observed. The length distribution of nanowires is random. After the thermal treatment process of heating the sample at 340ºC for 5 hours followed by gradual cooling for 4 hours, the average length of nanowires growing on the hillock is approximately 5 μm. As a result, the diameters of the nanowires fabricated by the thermal stress-induced method can be controlled by the thickness of the deposited Cu films, while the length of the nanowires only depends on the above mentioned heating and gradual cooling time. The aspect ratio of the as-obtained nanowires can be controlled by the proper management of the two factors.

In summary, it has been shown that nearly the thickness of Cu film can be used to define the diameters of nanowires fabricated by the stress-induced method.[64] Adjusting the thickness of the deposited Cu film is proposed to be the optimal way to fabricate nanowires with different diameters. Taking into account that the length of the as-obtained nanowires mainly dependent on the heating and gradual cooling time, the proper management of Cu film thickness and time can give rise to nanowires with controllable diameters and aspect ratios. It is worth mentioning the discovery, which the nanowire diameter fabricated by the stress-induced method can be tuned by adjusting the Cu film thickness, is important, since it is one of the simplest known means of fabricating controllable nanowires. Furthermore, this result would greatly broaden the possible applications of these nanowires for fabricating future nanodevices. It is believed that the

ability to exert a high degree of control over the diameter and aspect ratio of nanowires will facilitate the study of their fundamental properties and the exploration of their new applications in electronic, optical and optoelectronic nano-devices and sensors with high performance.

2.5 Component of as-obtained Nanowires

Nanowires are one-dimensional (1D) nanostructure with diameters down to a few nanometers and lengths up to tens of micrometers. The realization of these new classes of materials is primarily important for revolutionary advances in both science and technology. They provide a versatile platform for addressing fundamental questions in chemistry and physics at one-dimensional (1D) quantum size regime that is inaccessible in the past. In addition, enormous surface area and the size associated quantum confinement effect of these novel nanostructures make them unique and very attractive building blocks in bottom-up paradigm. Combined with novel device concepts and assembly techniques, conceptually new nanowire-based devices and device arrays can be developed, which could lead to new functions and/or greatly enhanced performance compared to conventional bulk/planar devices.

Characterization of nanomaterials plays a key role in understanding the properties of nanomaterials. This part focuses on the relevant methods used to characterize structural, morphological, and compositional properties of the samples made by the techniques

mentioned in the previous parts.

Electron microscopy is a technique of characterizing materials down to the atomic level, which has been serving as a powerful tool for analyzing and constructing new nanomaterials such as carbon nanotubes and nanowires. Electron microscopy can be broadly divided into two categories: Scanning Electron Microscopy (SEM) and Transmission electron Microscopy (TEM). The advancements in electron microscopy have revolutionized our understanding of nanomaterials by providing almost all of the structural, phase and crystallographic data.

To understand the fundamentals of electron microscopy, it is indispensable to know the basic principle of light optics. The limit of resolution is defined as the minimum distances by which two structures can be differentiated and still appear as two distinct objects. The limit of resolution is proved to depend on the wavelength of the illumination source. Due to diffraction and interference, a point of light cannot be focused as a perfect dot. Instead it forms an Airy disk. The radius of Airy disk is minimum distance of two objects can be distinguished from each other. Resolution in a perfect optical system can be described by Abbe's equation:

$$d = 0.612 \lambda / n \sin \alpha \cdot \qquad (2\text{-}1)$$

where d is resolution, λ is wavelength, n is index of refraction and α is the angle of the cone of light from specimen plane accepted by the objective. Therefore, optical microscopy has the limit of resolution of ~200 nm. For electron microscopy, the

illumination source and condenser lens in optical microscopy will be substituted with electron beam and electromagnetic coils. Emitted electrons from a source are accelerated at a high voltage (from several kV to 300 kV). Their wavelength is related to the accelerating voltage: $\lambda = h\,(2meV)^{-½}$, where V is the accelerating voltage, m and e are the mass and charge of the electron. The extremely small wavelength of electron (~0.04 Å at 90 kV) can push the resolution to atomic level.

Scanning Electron Microscopy (SEM) SEM complements optical microscopy for studying of microstructure texture, topography, and surface features with great clarity and detail. It can resolve morphologic details of less than 5 nm and possesses a depth of focus more than 500 times higher than that of the optical microscope at equivalent magnifications. Typical resolutions for SEM are around 10 nm. The combination of higher magnification, larger depth of focus, greater resolution, and ease of sample observation makes the SEM one of the most frequently used instruments in materials research today.

In SEM, electrons from the electron gun are focused to a small spot, 5 to 10 nm in diameter, on the sample surface and the electron beam scans the sample like the spot on a television screen. Most of the SEM operated at several to several tens kV and the resolution of a state-of-art field-emission SEM is around 5 nm. Image formation in SEM is dependent on the acquisition of signals produced from the electron beam and specimen interactions, shown in Figure 2.12.

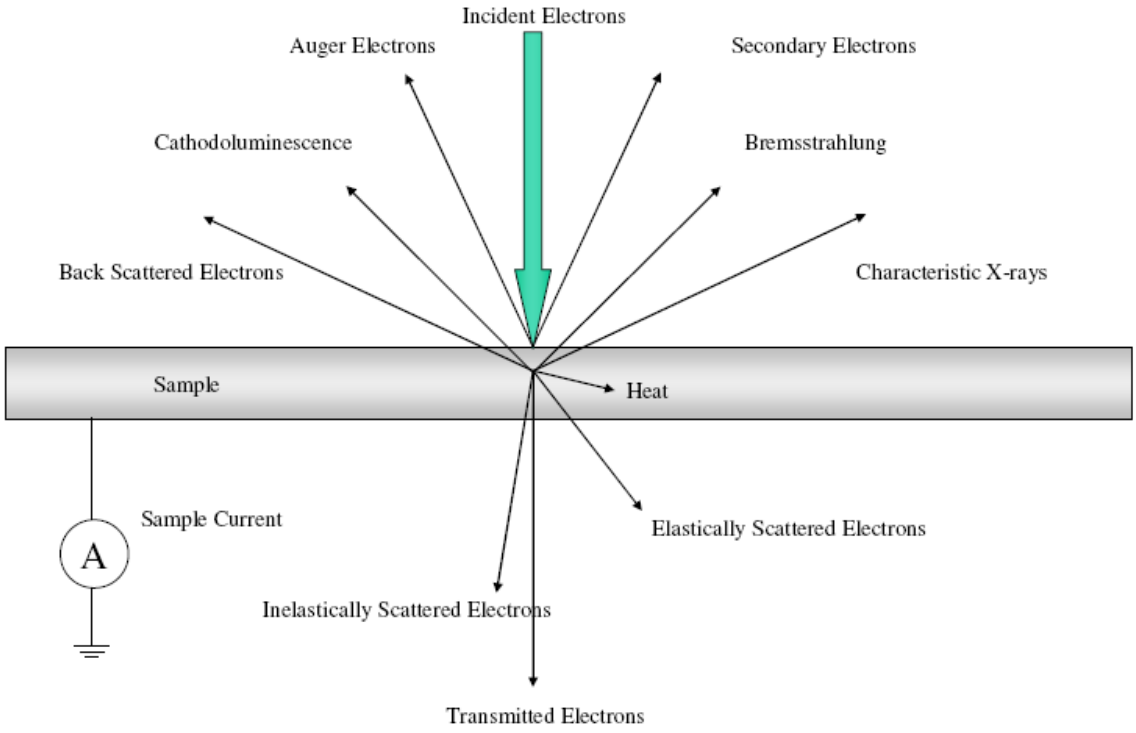

Figure 2.12 Signals generated when a high-energy beam of electrons interacts with a thin specimen.

The most widely used signal produced by the interaction of the primary electron beam with the specimen is the secondary electron emission signal. When the primary beam strikes the sample surface causing the ionization of specimen atoms, loosely bound electrons may be emitted and these are referred to as secondary electrons. Since the secondary electrons have small energy (several kV), the distance they can travel before reabsorbed by materials is around several nm. Therefore, secondary electrons accurately mark the position of the beam and give topographic information (e.g. surface texture and roughness) with good resolution. The penetration depth of electron beam depends on the

acceleration voltage.

The elastic collision between an electron and the specimen atomic nucleus cause the electrons bounce back with wide angle directional change, and this is called backscattered electrons. As expected, elements with higher atomic number have more positive charges on the nucleus, and as a result, backscattered signal is higher. Therefore, the contrast in backscattered electrons image is sensitive to the atomic number of imaged material. Due to the fact that backscattered electrons have a large energy, which prevents them from being absorbed by the sample, the region of the specimen from which backscattered electrons produced is larger than it is for secondary electrons. For this reason the lateral resolution of a backscattered electrons image is worse than it is for a secondary electron image.

Transmission electron Microscopy (TEM) TEM, as one of the most powerful tools in nanotechnology, has played an important role in characterizing one-dimensional (1D) nanostructures, not only in determining crystal and surface structure, but also chemical structure. As a result of those tremendous capabilities, TEM becomes the foundation of nanometer-scale technology. Figure 2.13 shows a schematic outline of a TEM. A TEM contains four parts: electron source, electromagnetic lens system, sample holder, and imaging system.

Functions of transmission electron microscopy (TEM) are similar to SEM, except the electrons are accelerated to 100 KeV or higher (up to 1 MeV), compared with 50KeV

maximum in SEM. The electron is a low mass, negatively charged particle. As such, it can easily be deflected by passing close to other electrons or the positive nucleus of an atom. These electrostatic interactions cause the electron scattering, which is the process to create TEM images and diffraction patterns. In comparison to SEM, TEM focuses on the transmitted electron signal. In order to get any information using TEM, the specimens have to be electron transparent (< 100 nm), depending on the density and elemental composition of the object and the resolution desired. Therefore, configurations and types of sample should be taken into considerations for choosing a suitable imaging technique.

It is noteworthy that TEM presents with 2D images of 3D specimens, not providing much information of the 3D view. All the TEM information is averaged through the thickness of the specimen. As a result of a high speed acceleration of the electron beam, elastic scattering phenomenon is observed as an ability of the beam to penetrate the thin piece of sample. Compared with SEM, a TEM can provide higher resolution imaging (0.1 nm) because it utilizes elastic scattering. The high magnification of TEM ranging from 50 to 10^6 is as well a result of such high speed electron beam. In addition, electron diffraction is an indispensable part of TEM and is arguably the most useful aspect of TEM for materials scientists. The solution of TEM is found to be in sub-nanometer range. Consequently atomic resolution (down to fractions of 100 pm) and magnifications of 50 million times can be achieved using a High Resolution Transmission Electron Microscope (HRTEM). HRTEM is capable of giving structural information on an atomic

scale, by direct lattice imaging and electron diffraction.

TEM diffraction pattern contains information on crystal structure, lattice repeat distance, and specimen shape, as well as being a most striking pattern.

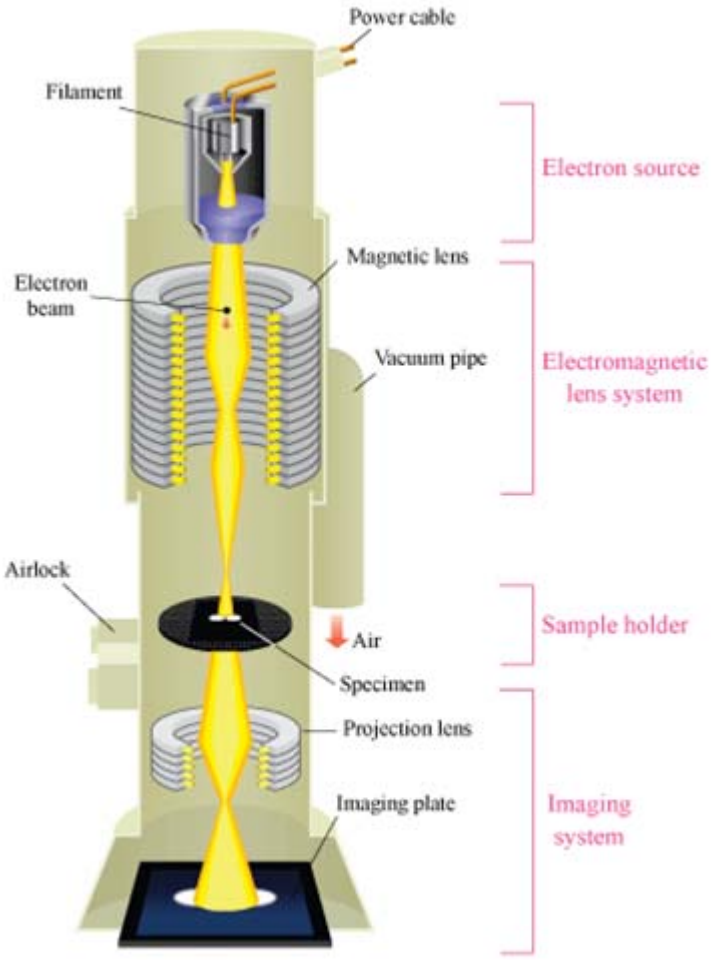

Figure 2.13 The schematic outline of a TEM.

Energy-Dispersive X-ray Spectroscopy (EDXS) Energy-Dispersive X-ray Spectroscopy (EDXS) makes use of the X-ray spectrum emitted a solid sample bombarded with a focused beam of electrons to obtain a localized chemical analysis. All

elements from atomic number 4 (Be) to 92 (U) can be detected in principle, though not all instruments are equipped for "light" elements (Z<10). Qualitative analysis involves the identification of the lines in the spectrum and is fairly straightforward owing to the simplicity of X-ray spectra. Quantitative analysis (determination of the concentrations of the elements present) entails measuring line intensities for each element in the sample and for the same elements in calibration standards of known composition. It is a measurement technique which relies on measuring the energy and intensity of emitted electro-magnetic radiation (light) to determine the chemical composition.[65]

By scanning the beam in a television-like raster and displaying the intensity of a selected X-ray line, element distribution images or "map" can be produced. Also, images produced by electrons collected from the sample reveal surface topography or mean atomic number differences according to the mode selected. The scanning electron microscope (SEM), which is closely related to the electron probe, is designed primarily for producing electron images, but can also be used for element mapping, and even point analysis, if X-ray spectrometer is added. This technique is performed in conjunction with SEM and is based on the interactions between electromagnetic radiation and matter, and on-destructive and has a sensitivity of >0.1% for elements. EDXS detectors cannot detect the presence of atomic number less than 5 elements because intensity of x-ray is very weak in light elements.

In this technique an electron beam of 10-20 keV strike the surface of a sample. The

electron beam can be precisely controlled and according to electron beam the EDXS spectra can be obtained either from a specific point/particle on the sample, giving an analysis of a few cubic microns of material or alternatively the beam can sweep over a selected area of the sample to identify the elements in that region. The bombarded electrons strike the specimen atom's electron resulting in some electrons being ejected and creation of a hole. This hole is eventually occupied by a higher energy electron from an outer shell and the excess energy of those electrons is released in the form of X-ray photons, shown in Figure 2.14.

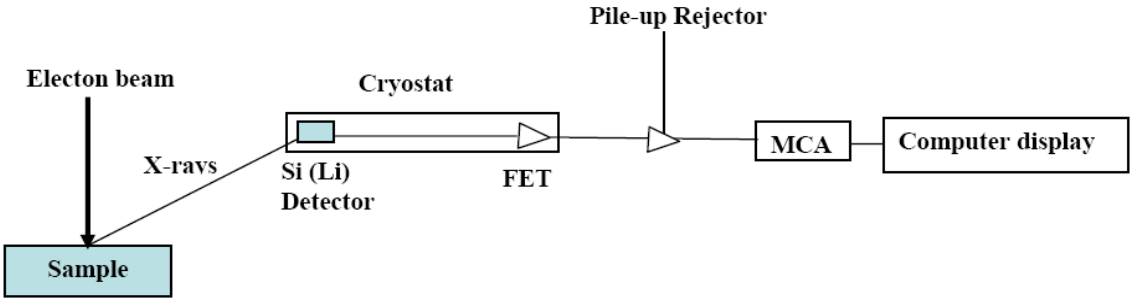

Figure 2.14 Schematic presentation of EDXS.

EDXS detector counts the ejected x-ray photon with respect to their energy. In the MCA (multi-channel analyser) the pulses are digitized and stored as pulse height spectrum. A spectrum of the kinetic energy versus relative counts of the detected x-rays is obtained in energy dispersive spectrometer. This spectrum is used to determine the qualitative and quantitative values of the elements present in the sampled volume. EDXS is not a surface science technique because X-rays penetrate the surface about 2 μm. In

addition, the area of interest can be defined by adjusting the size of the electron beam which can be as small as 5 nm diameter.

According to the typical EDXS, it can be operated in connection to SEM as an analytical tool for the elemental analysis of sample.

X-Ray Diffraction (XRD) X-ray diffraction, a result from the interaction between x-ray and materials, gives information about the structure of materials, such as the crystal phase, thickness and roughness of layered structures, grain size of polycrystals, texture and stress of samples, orientation and quality of single crystals, etc.

X-rays are electromagnetic waves with wavelength in the range from 10^{-12} m to 10^{-9} m. When a beam of x-rays interacts with a material with periodicity, such as a crystal, diffraction can happen if the wavelength of the x-ray is comparable to the lattice constant. A series of diffraction peaks can be detected at specific angles. Each constructive diffraction peak satisfies Bragg's law,

$$2d \sin \theta = n \lambda \qquad (2\text{-}2)$$

where n is the diffraction order, λ is the wavelength of the x-ray, d is the spacing between atomic planes, and 2θ is the angle between the incident and diffracted x-ray beams, as shown in Figure 2.15.

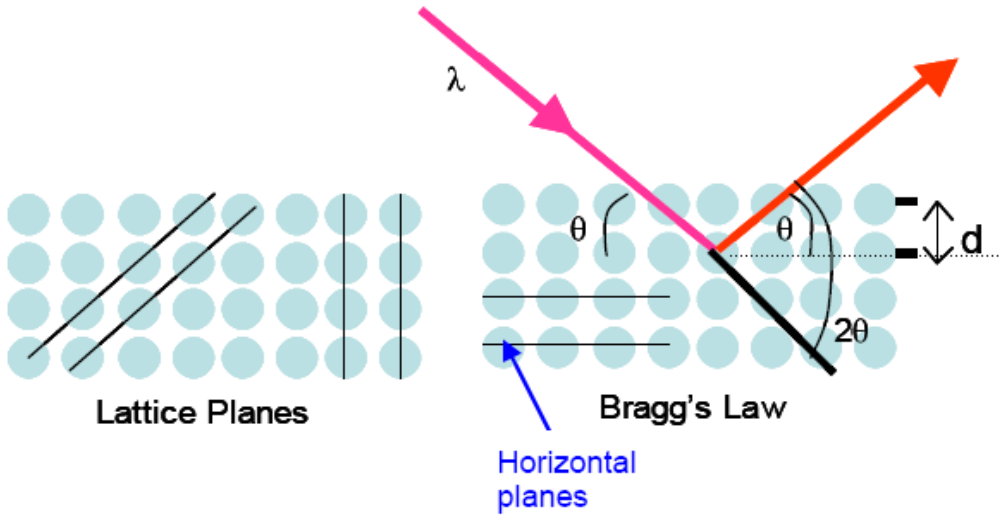

Figure 2.15 Schematic of x-ray diffraction in a crystal lattice with lattice constant d.

In the example shown in Figure 2.15, diffraction is only being measured from the horizontal planes of a crystal as function of 2 θ. For a complete analysis of a material, diffraction occurs at all the angles of 2 θ simultaneously in powder samples. In order to obtain a diffraction pattern, the detector (in most designs) rotates to various 2 θ angles to measure diffraction from the sample. Figure 2.16 is a schematic diagram for a powder X-ray diffractometer, showing the rotating detector.

Each material with a particular crystal structure has its distinctive diffraction pattern, which can be used to identify the structure of the material.

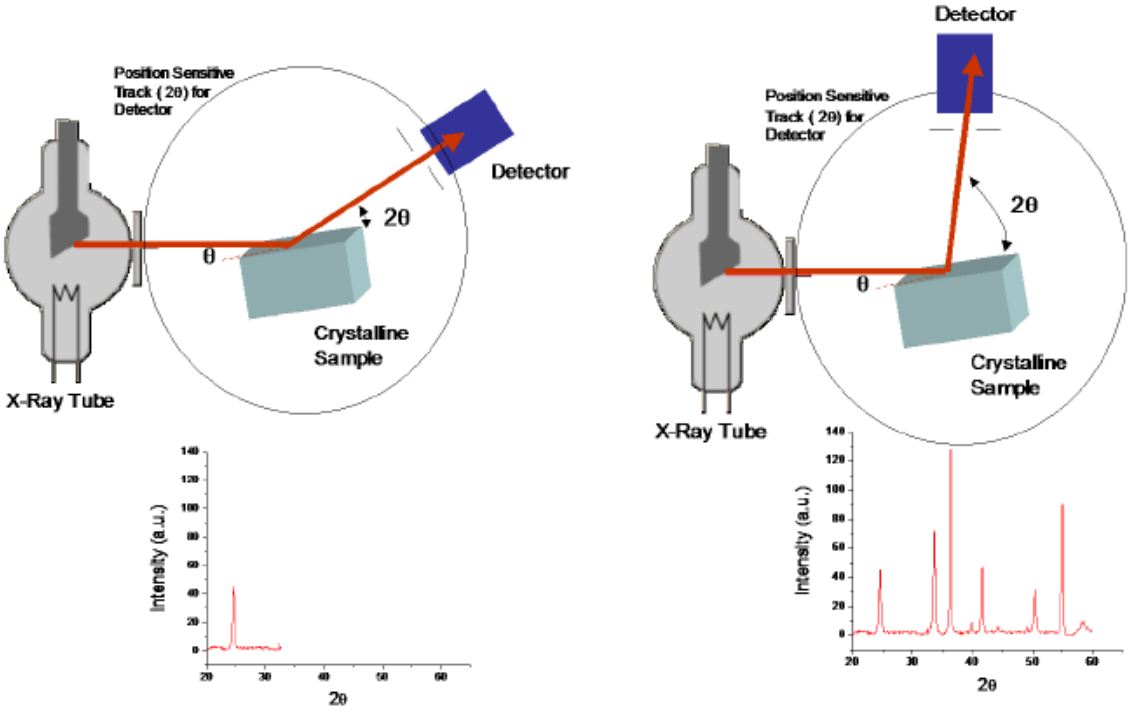

Figure 2.16 Schematic diagrams for a powder X-ray diffractometer.

The typical X-ray diffraction pattern contains a lot of information. From peak position，the space group symmetry, translational symmetry, and unit cell dimension may be determined and qualitative phase identification also can be made. Intensity of the peak may help to uncover unit cell contents and find the point symmetry. It is also capable to calculate crystal size, non-uniform micro-strain, and specify extended defects, such as stacking faults, twins, or anti-phase boundaries.

In this study, the morphology of the nanowires is firstly examined by SEM, which has been shown in the previous parts.

To further find out the feature of as-obtained nanowires of samples under optimum

growth condition, the samples with nanowires have been observed by the field emission scanning electron microscopy (FE-SEM). Here, high-magnification SEM image of a single nanowire on the substrate is shown in Figure 2.17. The SEM image recorded at high magnification clearly shows the perfect circular shape of the complete rings, with uniform and straight shapes. Obviously, the nanowire exhibits a smooth and homogeneous contour along its whole length. No change in diameter can be observed from the SEM image, indicating that the nanowire grows through continuous addition to its base, as opposed to possible thermal evaporation from the Cu film at high temperatures.

Quantitative analysis of the diameter from Figure 2.17 shows no significant change with starting and end diameters of approximately 33 and 30 nm, respectively. It means that the nanowire is uniform in diameter.

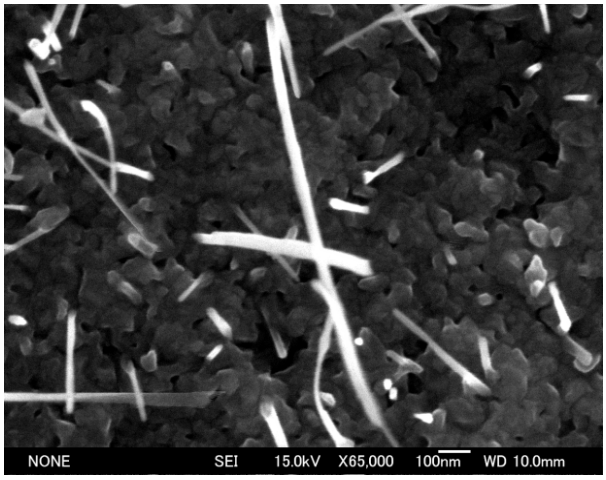

Figure 2.17 High-magnification SEM image of a single nanowire on the substrate.

To further find out the component and feature of as-obtained nanowires of samples, the samples with nanowires were also observed by energy dispersive X-ray spectroscopy (EDXS). The texture of the nanowires was analyzed by X-ray diffraction (XRD). Then, the fabricated nanowires were dispersed onto a Cu grid and observed by the transmission electron microscopy (TEM), selected-area electron diffraction (SAED) and high-resolution transmission electron microscopy (HRTEM) to further examine their microstructure and composition.

Figure 2.18 shows a TEM image of an individual nanowire from samples under the optimum growth condition. The individual nanowire from TEM image observation possesses cylindrical geometry and a smooth contour over the entire length with a resembling diameter, which is in good agreement with the above SEM results shown in Figure 2.17.

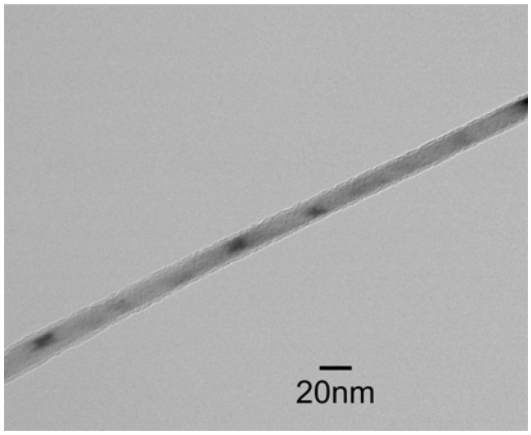

Figure 2.18 TEM image of an individual nanowire.

Therefore, it is especially important to point out that this method retains many of the

advantages of nanowire formation, namely, fast growth rate with uniformity in diameter, as well as high-quality crystal with control over size.

Figure 2.19 is a selected area electron diffraction (SAED) pattern taken from a random assembly of the nanowires under the optimum growth condition. From the SAED pattern, the compositions can be deduced to be Cu_2O and CuO, of which the former is the main composition.

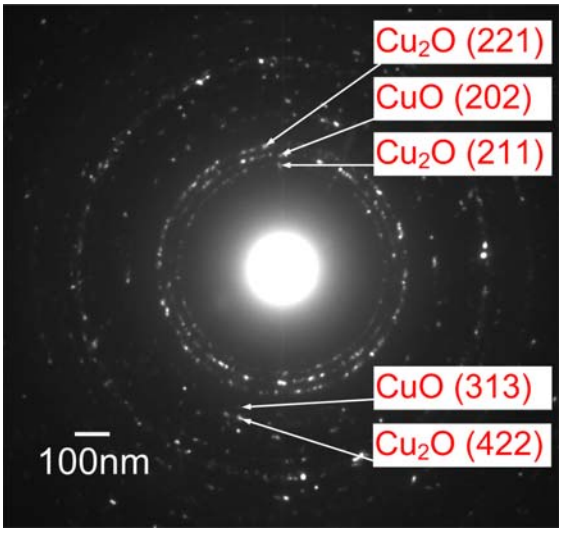

Figure 2.19 SAED image taken from a random assembly of the nanowires under the optimum growth condition.

In order to confirm the detailed inner structures and further structural investigation of an individual nanowire under optimum growth condition, a high-resolution transmission electron microscope (HRTEM) measurement is applied. Figure 2.20 shows the HRTEM image of a single crystal area with clear lattice fringes, demonstrating the high-quality single-crystalline of nanowires. The HRTEM image also indicates that nanowire

fabricated by the stress-induced method is structurally uniform. No defects, such as dislocations and stacking faults are observed. The lattice fringe spacing is about 0.304 nm, which corresponds to the {110} plane of Cu_2O crystal.

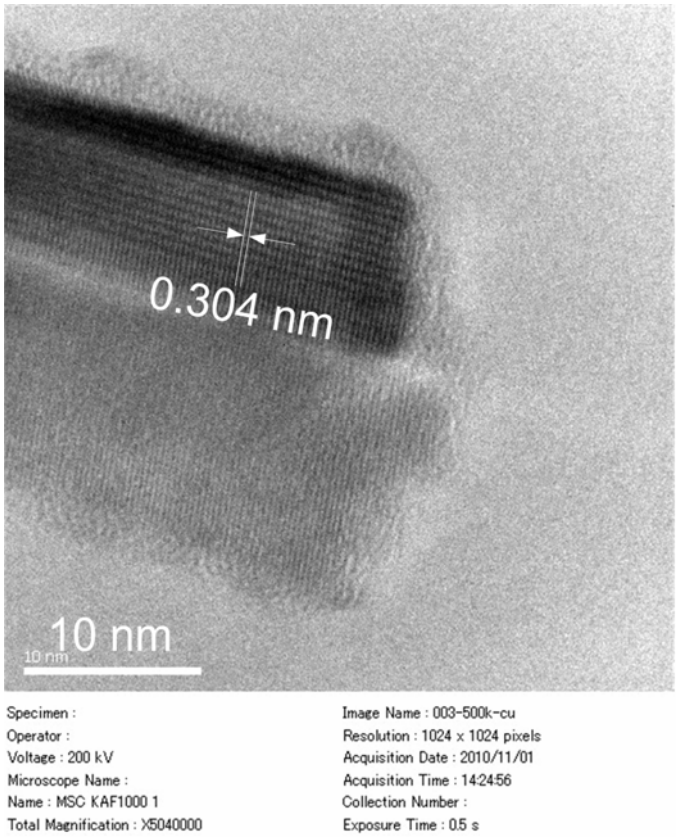

Figure 2.20 HRTEM image of part of an individual nanowire under optimum growth condition.

The chemical compositions of nanowires under the optimum growth condition have also been analyzed by the EDXS, as shown in Figure 2.21. The EDXS spectrum measured from the hillock surface of the sample indicates that the main chemical elements of the coated layer are Cu and O existing in the samples, the percentages of

which are 67.3% and 32.4% (nearly 2:1), respectively, consistent with Cu_2O formation. This result is in accordance with the SAED pattern shown in Figure 2.19 that the composition of the as-obtained nanowire is mainly Cu_2O. The presence of a small number of Ta elements shown in Figure 2.21 should originate from the Ta adhesion film which has been used during sample preparation, or is due to the migration of Ta atoms from the Ta adhesion layer.

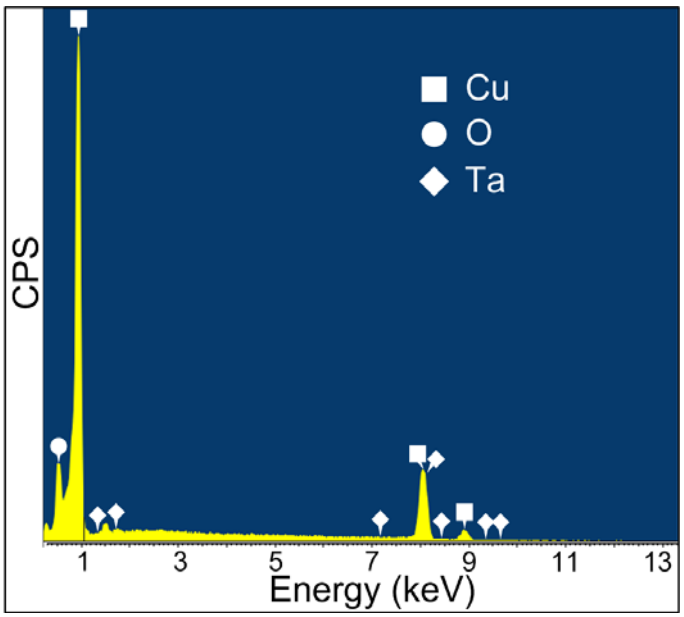

Figure 2.21 EDXS pattern taken from the surface of a hillock under the optimum growth condition.

XRD analysis on the surface of sample undergone the optimum growth condition, namely gradual cooling process, is shown in Figure 2.22 indicating the presence of both Cu_2O and CuO. But this figure also shows that the main composition of the sample surface and nanowires covering on it is Cu_2O, which matches the all above analysis

results quiet well.

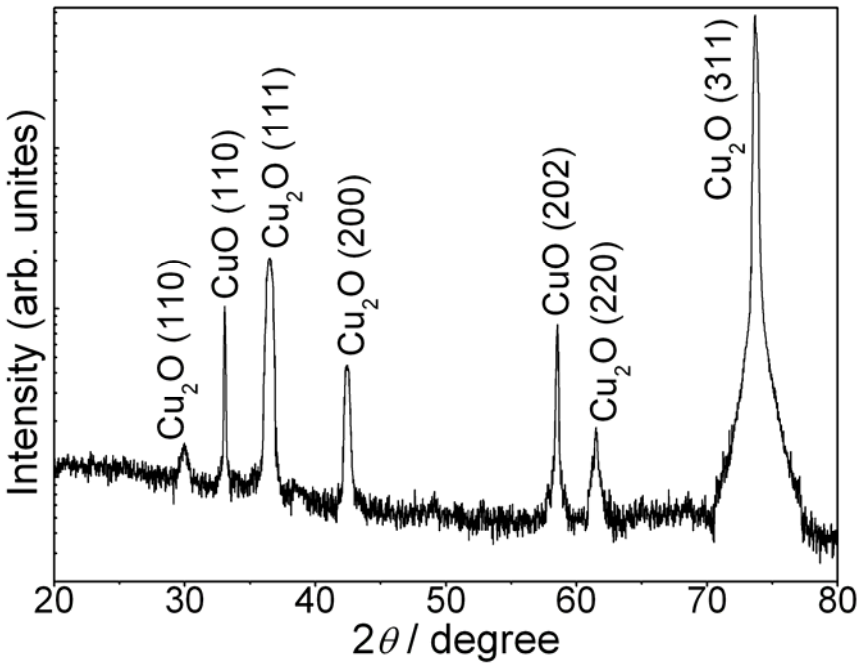

Figure 2.22 XRD analysis on the surface of sample undergone gradual cooling process.

To figure out the components of nanowires from different cooling process, namely direct cooling and gradual cooling process, X-ray diffraction (XRD) analysis has also been carried out on the surfaces of samples with direct cooling process, shown in Figure 2.23. The analysis on the XRD results indicates that the nanowires growing on the substrate from direct cooling process, which are generated in the heating process at 340°C, are mainly composed of CuO.

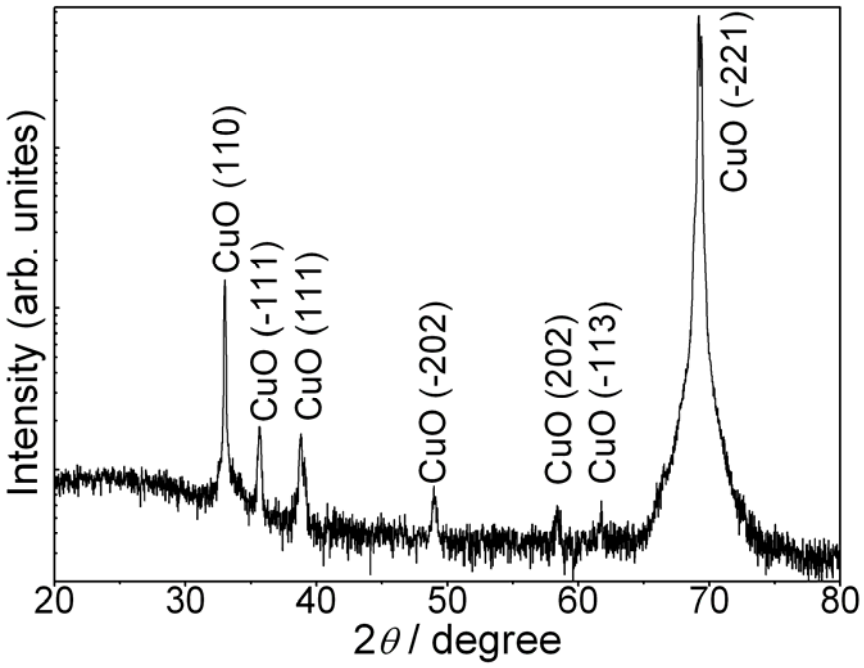

Figure 2.23 XRD analysis on the surface of sample undergone direct cooling process.

The nanowires collected from the direct cooling sample, have been also analyzed by HRTEM. The results are shown in Figure 2.24. The lattice fringe spacing in Figure 2.24 is 0.253 nm, which corresponds to the {002} plane of CuO crystal.

It should be noted that since Cu_2O is a metastable phase, some of the nanowires growing on the substrate which experienced the annealing process at 340°C may be further oxidized to be CuO. This is the reason why a few CuO, which should be the nanowires growing on the substrate, can be observed from sample even under gradual cooling process, shown in Figure 2.19, 2.21 and 2.22. Since the hillocks and nanowires on them are generated during the gradual cooling process at relatively low temperatures, the main component of them is demonstrated to be Cu_2O, as also shown in Figure 2.19,

2.21 and 2.22, and they can hold the metastable phase of Cu_2O. However, Cu_2O nanowire can be hardly observed from the direct cooling sample shown in Figure 2.23.

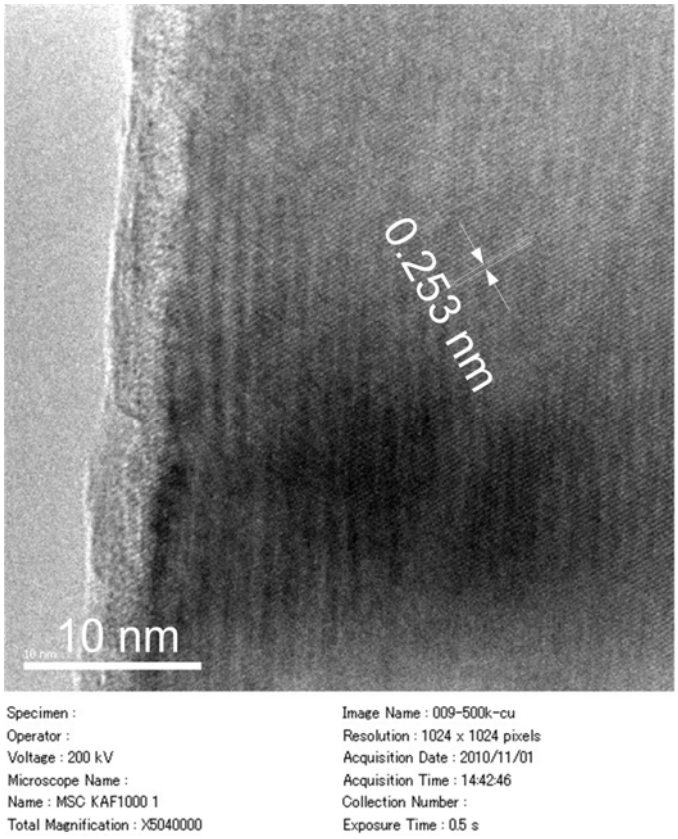

Figure 2.24 HRTEM image of part of an individual nanowire under direct cooling process.

The X-ray diffraction (XRD) results (shown in Figure 2.22 and 2.23) and high-resolution transmission electron microscopy (HRTEM) results (shown in Figure 2.20 and 2.24) on samples with direct cooling process and gradual cooling process indicate that nanowires growing on the substrate are mainly composed of CuO, while nanowires growing on the hillocks are mainly composed of Cu_2O. These results further

demonstrate that the gradual cooling process is of great significance in fabricating Cu_2O nanowires.

In summary, large-scale Cu_2O nanowires on deposited Cu thin films have been fabricated by the stress-induced method with creatively laying stress on the cooling process, without employing any templates, any catalysts and vacuum system. The optimum growth condition of heating for 5 hours at 340°C and cooling gradually for 4 hours is first proposed. The as-obtained Cu_2O nanowires are mainly single-crystal and defect-free ones with smooth surfaces and uniform cross-sections along their axes. Moreover, these Cu_2O nanowires own larger aspect ratio and higher growth density.

XRD and HRTEM analysis on samples with direct cooling process and gradual cooling process have demonstrated for the first time that the gradual cooling process is of great significance in fabricating high-quality Cu_2O nanowires.

Control of the diameter of Cu_2O nanowires has been come true in a simple and accessible manner. The thicknesses of the deposited Cu films could be varied to adjust the diameter of nanowires, and the proper management of Cu film thickness and the heating and gradual cooling time can give rise to Cu_2O nanowires with controllable diameters and aspect ratios. These results provide a step toward the controlled growth of Cu_2O nanowires.

To the best of our knowledge, fabrication of Cu_2O nanowires with high-yield and high-quality by the stress-induced method has not yet been reported elsewhere.

Chapter 3 Analysis of Growth Mechanism

Any new phenomenon requires new explanation and deep understanding. Here, the new challenge comes with the advent of the new phenomenon mentioned in the previous chapter in this dissertation research.

In fact, the demand for the stress-induced method becomes increasingly important as Cu_2O nanowires have emerged as attractive candidates for high efficiency semiconductor materials where the crystallinity of the nanowires needs to be exceptionally high. In this regard, an attempt to identify the growth mechanism, which expands the range of materials readily available for fabrication by the method, must be investigated. Fundamental and overall understanding of the growth process is critical for the fabrication of Cu_2O nanowires with a good control of the atomic precision morphology, structure, and size, so as to enable precise control over the properties of the resulting nanowires. Moreover, it is also of extreme importance to further fabricate quality control of nanowires and modification of the processes as needed. However, present knowledge about the growth mechanism of Cu_2O nanowires in the research is still quite limited.

Herein, the objectives of this chapter are to conceive more accurate growth mechanisms involved in the optimum growth condition, and the detailed studies should been undertaken to develop a better understanding of the new phenomenon about nanowire growth and hillock formation. A major and important task but the real

challenge would be the modification of nanowires quality and some properties in order to adapt them to the required more applications.

Before analysis of growth mechanism in the dissertation research, well-accepted nanowire growth mechanisms are described in detail as follows.

As mentioned previously, the essence of forming nanowires is crystallization from vapor, liquid or solid phases. For nanowire synthesis, two primary growth mechanisms of the nucleation and growth are widely accepted amongst the nanowire synthesis community: the vapor-solid (VS) process[66] and the vapor-liquid-solid (VLS) process.[67]

Vapor-Solid Process During a catalyst-free vapor-solid (VS) growth process, deposition occurs when vapor condenses directly to form a solid without experiencing an intermediate liquid phase. In a typical VS process, the vapor species is firstly generated by evaporation, chemical reduction, laser ablation, and other gaseous reactions. These species are subsequently transported and condensed on the surface of a solid substrate placed in a zone with lower temperature than that of the source materials. As a consequence of the research on VS process, whiskers naturally growing are thought to be kinetically-driven, anisotropic, crystallization processes that are heavily dependent on supersaturation.[8] Fortunately the temperature and the supersaturation ratio are easily controlled parameters during synthesis. In a word, temperature and the supersaturation ratio are the two dominant factors during VS growth and provide the ability to control the morphology of deposited product.

The vapor-solid (VS) growth process is illustrated in Figure 3.1. The source materials is vaporized into molecular species at high temperature and transported downstream by carrier gas. At the low temperature region, the vapor is condensed onto the substrate, as shown in Figure 3.1 (a). During the condensation, the cation-anion molecules arrange in such a way that the proper cation-anion coordination is preserved to balance the local charge and structural symmetry, forming a small nucleus, as shown in Figure 3.1 (b). Newly arriving molecules continue to deposit on the formed nucleus while the surfaces with lower energy start to form the side surfaces. Because of the local growth temperature, the mobility of the atoms/molecules is high enough that the low-energy surfaces tent to be flat, preventing the transverse growth normal to the side surfaces, as shown in Figure 3.1 (c). The side surface expands as more molecule stick onto the rough growth front, leading to the fast growth of a nanowire and formation of long nanowire, as shown in Figure 3.1 (d) and (e). The size of the nanowire is determined by the growth temperature and supersaturation ratio in the kinetics of crystal growth. Therefore, the VS growth can be considered as starting from “self-catalytic” initiation.

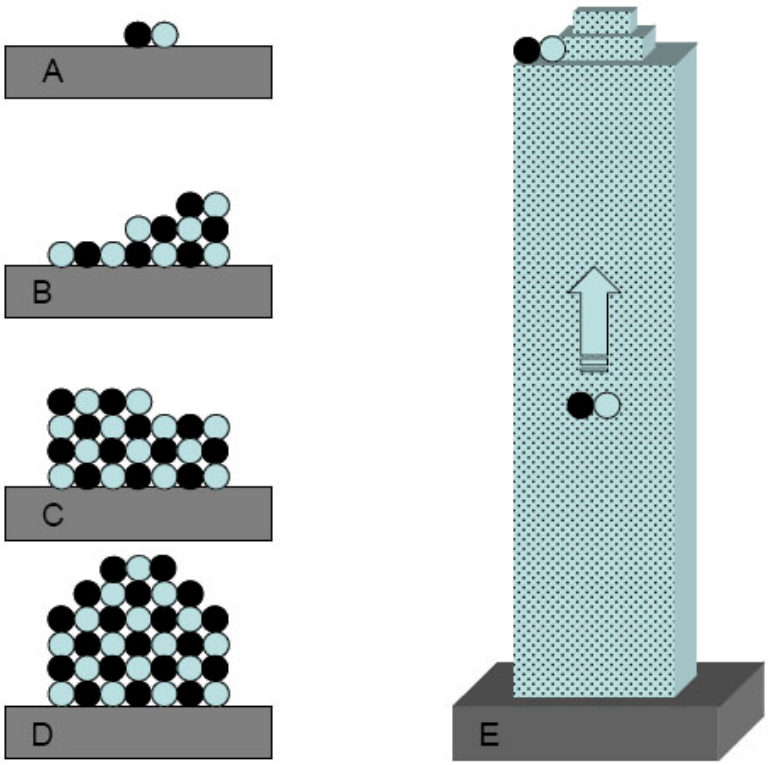

Figure 3.1 Schematic steps of the nanowire growth via VS process.

Vapor-solid growth of nanowires is historically based on whisker formation, and the whisker had been firstly observed as early as in 1946.[68] Although the exact mechanism responsible for nanowire growth directly from the vapor phase is still not fully understood, this approach has been explored by many research groups to synthesize nanowires from a variety of materials. As early as 1950s, it was reported that acicular structured oxides of metals such as Cu, Cr, Fe, Pb, Ti, W, and Zn could be produced on the external surfaces of the corresponding metals when they were heated in air at certain temperatures.[69] Now it is generally accepted that the control of supersaturation is a prime consideration in obtaining nanowires.[8]

Vapor-Liquid-Solid Process In VLS mechanism,[70] a catalyst serves as a nanocluster or nanodroplet that defines the diameter of a growing nanowire and serves as the site that preferentially directs the addition of reactants to the end. It readily provides the intellectual underpinning needed for the specification of the catalyst and growth conditions required for predictable nanowire growth. The equilibrium phase diagrams are used to determine catalyst materials that form a liquid alloy with the nanowire materials of interest. The phase diagram is then used to choose a specific composition and growth temperature such that there is a coexistence of a liquid alloy and a solid phase. Therefore, this temperature is normally limited to the range between the eutectic temperature and melting point of nanowire materials. The liquid catalyst alloy cluster serves as preferential site for absorption of reactants since the sticking coefficient is much higher on liquid surface than on solid surface. Once the liquid catalyst alloy cluster is supersaturated, the nucleation site starts crystallization. Preferential nanowire growth occurs in the presence of reactants as long as the catalyst nanodroplet remains in the liquid state. Within this framework, it is straightforward to synthesize nanowires with different diameters and compositions, if appropriate nanoscale catalyst clusters are available.

The vapor-liquid-solid (VLS) growth process is illustrated in Figure 3.2. With the existence of material vapor, the solid metal nanoparticles, as shown in Figure 3.2 (a), form liquid alloy droplets once the deposition temperature rises above the eutectic

temperature of the metal and material, as shown in Figure 3.2 (b). The incoming material vapor causes the percentage of the material component in the droplet to increase and ultimately supersaturates. The material is precipitated out at the solid-liquid interface, as shown in Figure 3.2 (c), and growth continues until the source vapor is cut off or the temperature drops below its eutectic point, as shown in Figure 3.2 (d).

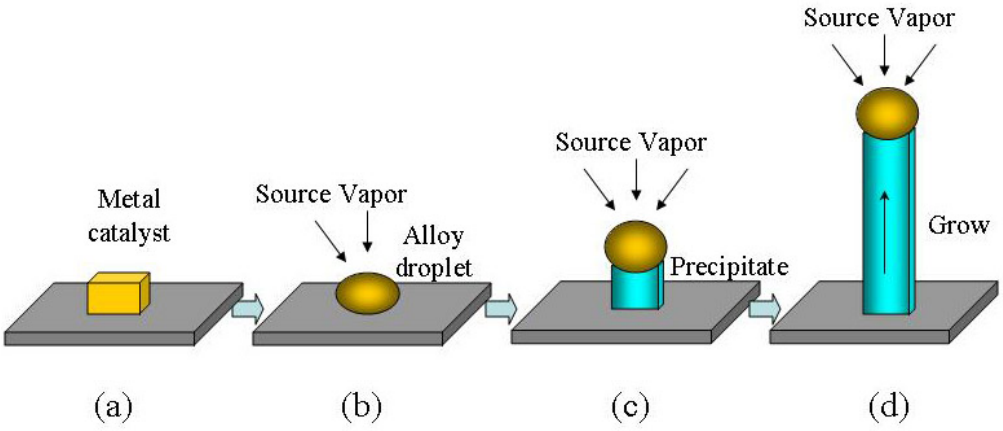

Figure 3.2 Schematic steps of the nanowire growth via VLS process.

The VLS growth mechanism has been studied extensively and become the most successful approach for generating single-crystal nanowires in large quantities.[12, 71]

Compared to VS process, the mechanism of VLS process is much better understood.

Moreover, other than VS and VLS growth mechanism, many other growth mechanisms have also been proposed for the synthesis of nanowires, such as solution-liquid-solid (SLS),[72] oxide-assisted growth mechanism[73,74,75] and vapor-solid-solid (VSS) mechanism.[76, 77, 78, 79] These other mechanisms might also play an important role in certain synthesis process.

According to the category of nanowire growth mechanisms, these as-obtained nanowires in the dissertation research have clean tips shown in Figure 3.3, unlike the reported metal-seeded VLS growth techniques, which normally have a metal ball at the tip of the nanowires. Intuitively, the vapor-solid process seems to be able to better explain the growth of nanowires in the present study. Thus, this nanowire growth by the stress-induced method is supported by the VS process, where grains on the film only served as the nucleation sizes to initiate the nanowire growth.

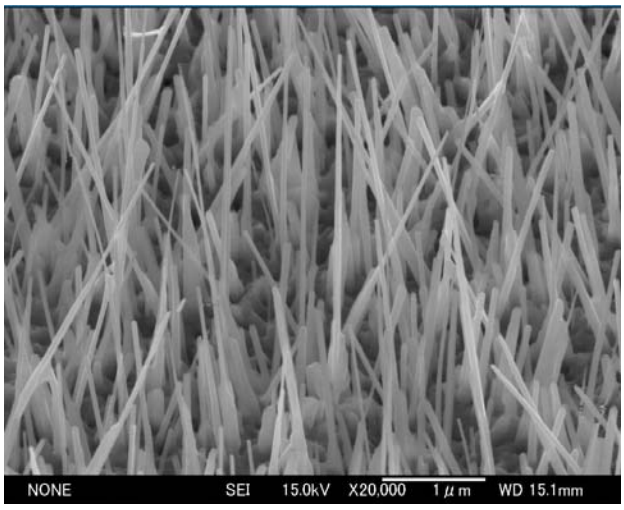

Figure 3.3 SEM image of nanowires with clean tips.

3.1 Stresses in the Cu Film

These direct observations provide experimental evidence that clarify the driving force for nanowire growth.

When the Cu/Ta/SiO_2/Si structure was fabricated and placed in air at room temperature, there was almost no stress in all the layers. Then the top of Cu film was oxidized in the

atmosphere at room temperature to form a thin layer of Cu_2O. When the $Cu_2O/Cu/Ta/SiO_2/Si$ system is heated to about 340°C, all layers in the system will experience thermal expansions (for Cu_2O maybe contraction) due to their different thermal expansion coefficients, as shown in Table 3.1. If the material parameters shown in Table 3.1 are taken, the stress in each layer can be roughly estimated. To keep the deformation compatibility of the whole system, circumferential tension or compression stresses occurs in all layers.

Table 3.1 The material parameters

Material	Thermal expansion coefficient ($10^{-6}K^{-1}$)	Young's modulus (GPa)	Poisson's ratio	Thickness (nm)
Si	2.6 at 25°C	130	0.28	2.8E5
SiO_2	0.5	~70	~0.17	300
Ta	6.3 at 25°C	186	0.34	60
Cu	16.6 at 25°C	110-128	0.34	416
Cu_2O	-8~-3 (-5)	82±12	0.5	~10

In brief, the Cu thin-film on the substrate is in a stressed state due to different thermal expansion of all layers. The Cu thin-film expands when it is annealed, while the substrate restricts expansion, putting the Cu film under compressive stress. Then a significant

change in geometry may occur. Bending moment in thin multi-layer film arises due to unbalanced in-plane stress in the top and bottom layers of the film. The explanation process is shown in Figure 3.4. The deformation can be converted into the film stress by appropriate mechanics using known material properties and geometrical dimensions of the film and the corresponding substrate.

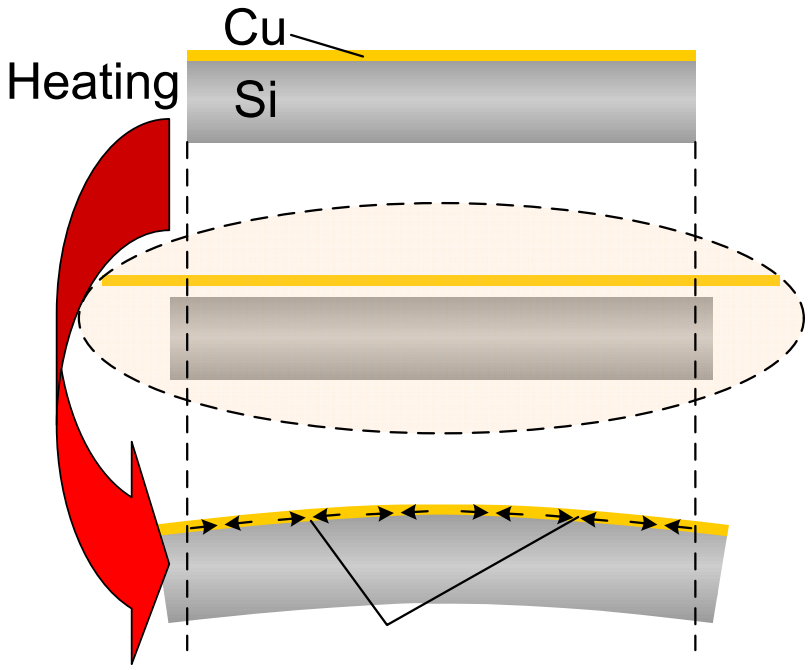

Figure 3.4 Schematics for the growth of nanowires: The compressive stresses generated in the Cu film by heating.

Measurements of the stresses in the Cu thin-film are of great importance in terms of analysis of growth mechanism. Therefore, the accurate measurement and analysis of the film stresses associated with heating and gradual cooling process is necessary to

understand appropriately the nanowire and hillock growth mechanism for further fabricating quality control of nanowires and improvement of the processes. This study is to examine the additional thermal effects of certain processing techniques on substrate deformation and film stress, further nanowires and hillocks growth.

Since stress cannot be measured directly, modeling of actual stress that occurs in thin-films is extremely difficult. Analytical and experimental methods have been developed in order to better understand stresses in the Cu thin-film. Therefore, curvature information is needed to accurately determine the film stresses.

The easiest and probably most common method to determine film stresses in a thin-film on substrate system due to some process is to measure the substrate curvature of the system before and after a specific process, and apply appropriate relations that connect curvature to stresses in order to determine the film stresses from the specific process. The resulting change in curvature then can be directly related to the film stresses caused by the specific process. The classical relation between film stresses and substrate curvature in the overlying thin-film on the substrate is known as the well-known Stoney's formula, usually used as in a uniform, homogeneous thin film on a much thicker substrate.[80]

First such work was that of G. Stoney investigated stresses in metallic films deposited electrolytically. Over the years, many extensions to the Stoney formula have been derived by various researchers who have relaxed different assumptions made by the original

Stoney analysis. It have been extended to more complicated structures such as multi-layer structure,[81] unpassivated line structures,[82] and passivated line structures.[83]

In this part, a theoretical analysis for curvature evolution in the Cu thin-film on a silicon substrate is proposed. The stress change in the 400 nm thick Cu thin-film was measured by means of a substrate curvature system using a two-dimensional laser array deflected from the sample during heating from room temperature to 340℃ and during gradual cooling process for 4 hours. The stresses in the Cu film were derived from the measured curvature using Stoney's formula.

Theoretical Background The Stoney formula is still widely applied. Also, the variations between film stresses of the different thin film-substrate geometries are examined. The Stoney formula was derived based on several explicit assumptions. The main assumptions are (i) both the film thickness and substrate thicknesses are small compared to the lateral dimensions; (ii) the film thickness is much less than the substrate thickness; (iii) the substrate material is homogeneous, isotropic and linearly elastic, and the film material is isotropic; (iv) edge effects near the periphery of the substrate are inconsequential; (v) all physical quantities such as Young's modulus and Poisson's ratio are invariant under change in positions parallel to the interface; (vi) all stress gradients in the thickness direction vanish throughout the material and (vii) the strains and the rotations are infinitesimally small.

The thin-film stress is determined from Stoney's formula, that is,

$$\sigma_f = \frac{1}{6}\frac{E}{1-\nu}\frac{t_s^2}{t_f}\frac{1}{R}$$
$$= \frac{1}{6}\frac{E}{1-\nu}\frac{t_s^2\lambda}{t_f r^2}\Delta N \quad (3\text{-}1)$$

In equation (3-1), σ_t is the average thin-film stress, E is the Young's modulus of the substrate, v is the Poisson's ratio of the substrate, t_f and t_s are thicknesses of the film and the substrate, respectively. R is curvature of film-substrate system. r is film diameter, and λ is laser wavelength. ΔN is the stripe number. The average is used because in most cases, one scan across the substrate is not sufficient. These simplified relations are then integrated to find the relationship between substrate deformation and film stress.

This technique determines the individual material film stresses, and to find a composite value, a volumetric average is taken. The technique is also developed to identify system parameters and to characterize stresses induced by deformation in the thin-film. In the research, substrate and film refer to Si and Cu film, respectively.

Table 3.2 shows some material properties used in the analysis.

Table 3.2 Some material properties

Material	E(GPa)	v	α (10^{-6}/℃)
Si	130	0.28	2.60
Cu	110	0.30	17.0
SiO_2	71.4	0.16	0.524

With the given material properties and geometrical dimensions of a film–substrate system, the measured curvature can be converted into the film stresses by using the Stoney formula.

This simple equation, based on small deformation theory, enables the calculation of film stresses without knowledge of properties of the thin film, and has been used widely in a variety of applications where a uniform film is deposited on a thicker substrate and modified to extend up to multilayer structures with or without compositional gradients.

So far, a methodology which is able to determine film stresses has been introduced. Since this methodology requires knowledge of curvature information over the entire wafer, a full-field curvature measurement technique is also introduced as follow.

Experimental Setup and Method For the deflection curvature in this dissertation research, a laser measurement system is set up to measure the deflection curvature of the multi-layer substrate under thermal change. The set of equipments is suited to the analysis because it can produce curvature information over the entire wafer surface, which is required for this analysis. The deflection measurement setup is illustrated in Figure 3.5. The deflection curvatures can be obtained via the system.

The film samples are multi-layer substrates mentioned in chapter 2.1.

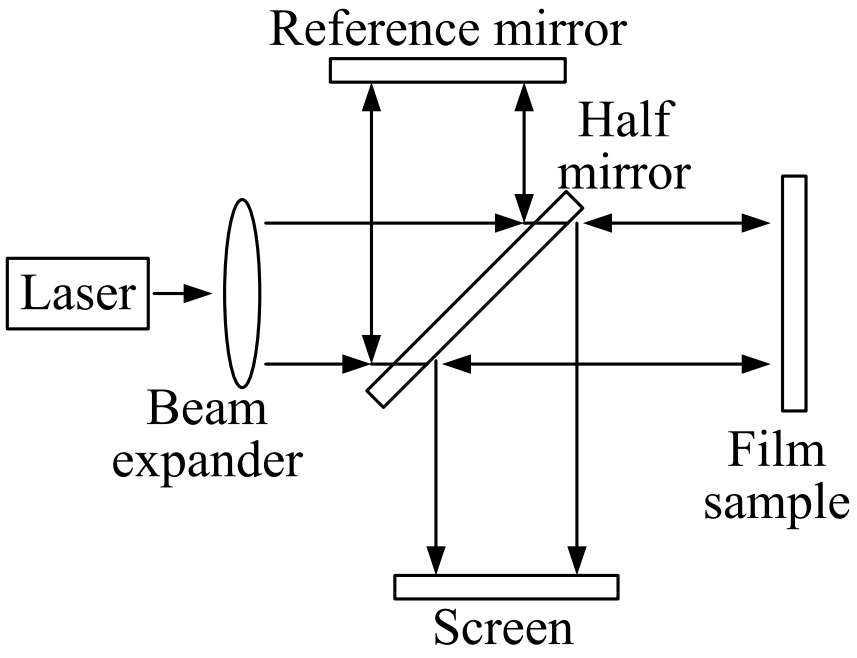

Figure 3.5 Schematic diagram of curvature measurement experimental setup.

The detailed explanation can be followed using Figure 3.5. In the setup, a monochromatic 632.8 nm-wavelength beam of laser light is emitted by a laser source, through a beam expander, to a mirror that functions as a half mirror. From here, the half mirror splits the incoming light into two identical beams along perpendicular paths, which directs it down to the film sample surface at near-normal incidence. That is, one beam is reflected by a screen positioned at a fixed distance from the half mirror, and the other is reflected by the film sample surface, which is reflective at its wavelength of light. Once reflected from the film sample surface, the light follows the same path in reverse until it reaches the half mirror which is located in the center of the figure. The portion of the

reflected beam that is deflected by the half mirror (rather than passing through it) is then reflected by another screen. The split beams recombine at the half mirror, and the recombined beam subsequently passes through the half mirror and is collected down on the reference mirror, where focuses the two combined beams on one spot. Finally, the resulting interference fringes are recorded by a CCD camera positioned on the reference mirror and imaged by a television monitor. The bulged film sample induces phase differences in the recombined beam, which creates interference fringes in the image. Due to the hemispherical shape of the deflected film, the interference fringes take the form of concentric rings.

In general, to determine stresses from measurements, interference fringes are taken before and after the heating process, and the different interference fringes are used to obtain curvature maps, and then film stresses through the stress/curvature relations as described in above section.

The images in Figure 3.6 illustrate the typical interference fringes observed during heating process and gradual cooling process.

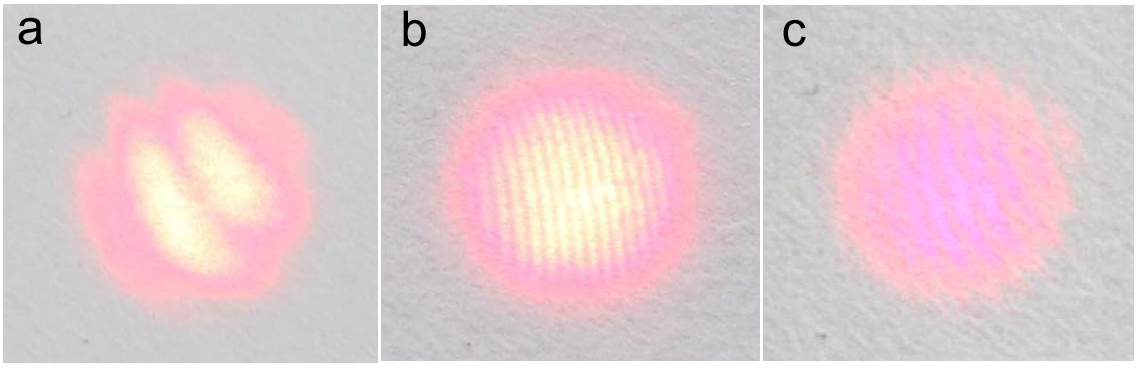

Figure 3.6 Interference fringes measured on Cu thin-film: (a) before heating process, (b) during the heating process (at 120 °C), and (c) after the heating and gradual cooling process (at 130 °C).

Extracting Stresses from interference fringes Interference fringes, obtained from the above experimental setup, are then used in conjunction with the Stoney methodologies to determine film stresses in the Cu thin film, which can be derived from the interference fringes measured by the laser interference method using Stoney's formula (3-1). The substrate thickness is approximately 1.8 μm, and the diameters are approximately 20 mm. The Young's modulus of in-plane Si substrate is 130 GPa, and the Poisson ratios is 0.28, respectively. The heating and gradual cooling process, namely the optimum growth condition, is performed in this part. The substrate is expected to incur deformation due to thermal effects. The result of macroscopic stresses over the all Cu film during the special process is shown in Figure 3.7.

Figure 3.7 shows the variation of biaxial stresses in the 400 nm Cu film as a function of temperature between 25 and 340 ℃. Note the *y*-axis is the change in stress, not the

absolute stress. From the Figure 3.7 observation, in the early stage of heating process, the stress begins to decrease and becomes more compressive stress because of the thermal expansion mismatch of different layers, and then remains nearly constant with further increasing temperature. During isothermal annealing at 340℃, the stress decreases by relaxing the compressive stress for nanowire growth. The compressive stress continues to be relieved for hillocks and nanowires growth during cooling process, and finally becomes tensile stress.

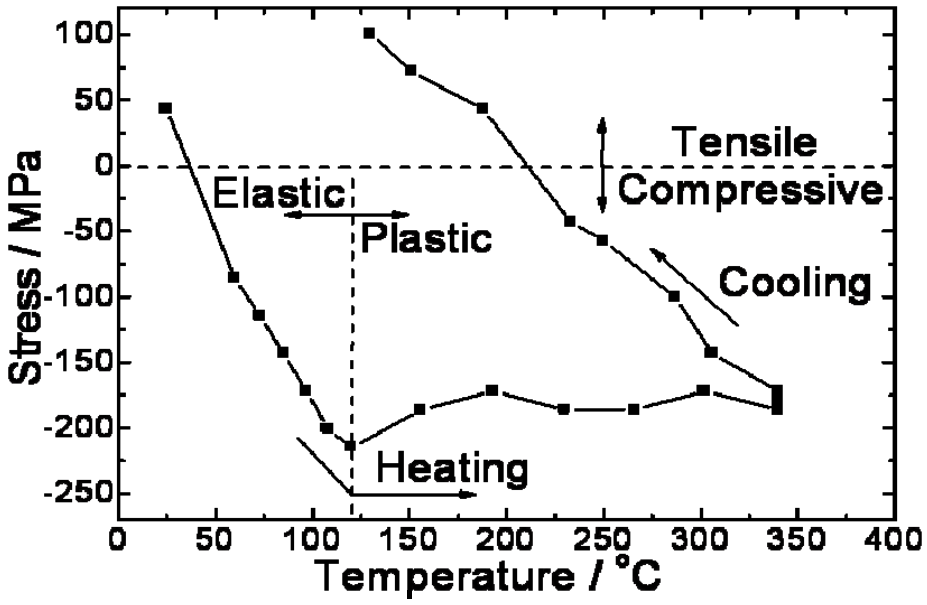

Figure 3.7 The macroscopic stresses over the whole Cu film measured by laser interference during the heating and gradual cooling process.

3.2 Heating Process

The heating process is illustrated in Figure 3.8. During the heating process, the

temperature is kept at 340°C. In its early stage, due to the stress gradient between the oxide layer and the oxide layer/Cu film interface, the Cu atoms are accumulated by surface diffusion at first. The surface diffusion of Cu atoms near the oxide/Cu interface is caused by the stress concentrations which occur at the grain boundaries due to material singularities. However, the continuous surface diffusion of atoms leads to a lack of Cu atoms around the grain boundaries and the local accumulation of Cu atoms on the grains near the interface, and as a result, the gradient of the local stress is reduced. Then, the Cu atoms are supplied continuously by grain boundary diffusion in the direction of the film thickness to the grain boundaries where they are lacked due to preceding surface diffusion. When the diffusion rate is high enough and the accumulation of Cu atoms at the oxide/Cu interface attains a critical value, the accumulated Cu atoms start to penetrate the oxide layer via any weak spots of the layer, and then the nanowires are nucleated. The growth of Cu nanowires continues in a relatively low rate. The growth of nanowires relieves part of the compression stress in the Cu film near the oxide/Cu interface. As a result, the stress gradient between the oxide layer top and the interface become smaller. In other words, the stress gradient between the top (oxide side) and bottom (Si side) faces of the Cu film is generated.

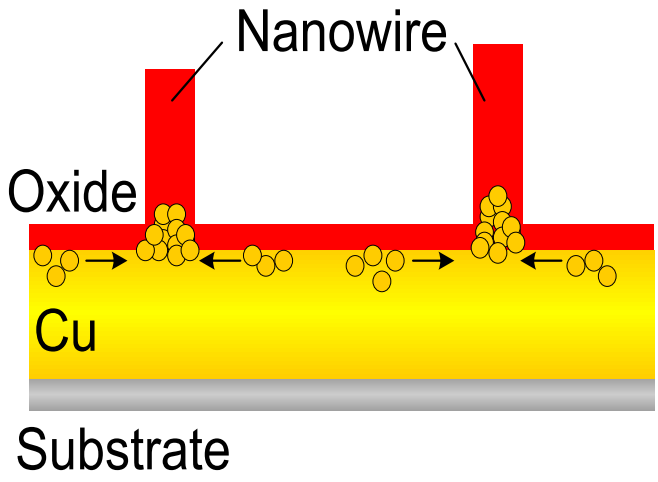

Figure 3.8 Schematics for growth of nanowires on the substrate.

3.3 Cooling Process

The cooling process is illustrated in Figure 3.9. During the gradual cooling process, the stresses induced in the sample due to the thermal expansion tend to disappear, and the sample tends to recover to the state before it is heated. However, since the growth of nanowires during heating process has relieved a lot of the compression stress in the Cu film from the oxide/Cu interface, a local tensile stress is generated in the Cu film near the oxide/Cu interface in the contraction process of the Cu film. Consequently, a larger stress gradient is formed between the top (oxide side) and bottom (Si side) faces of the Cu film, which might further increase the diffusion rate of Cu atoms moving from the bottom to top faces of the Cu film. As a result, a huge diffusion of Cu atoms is realized, the formation of hillocks occurs.

When the growth rate of hillocks is too high, which corresponds to a relatively high

cooling rate, the formation of surface oxide layers can't catch up with the growth of hillocks, and thereby little nanowires grow on the hillocks. When the cooling rate is too low, the stress gradient might not be large enough for the rapid diffusion of Cu atoms, and the growth of hillocks can't match with the formation of thick surface oxide layer, thereby, fewer nanowires can be obtained. Only when the gradual cooling rate is held in a proper rate, dense and long nanowires can grow on the hillocks.

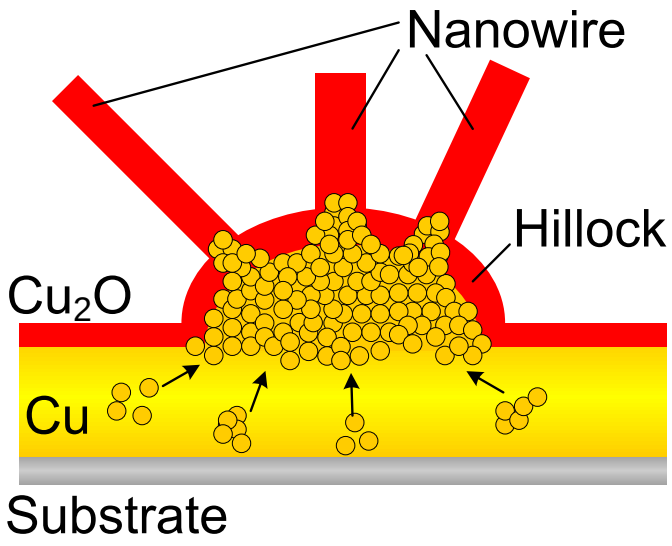

Figure 3.9 Schematics for growth of hillocks and nanowires on them.

On the other hand, when the sample is cooled directly, more cracks instead of hillocks are formed on the sample surface due to the extremely high cooling rate.

This analysis in this part is in good agreement with the experimental results in the research, and it is also the correct explanation for the optimum growth condition

proposed in Chapter 2.3.

In summary, the stresses in the presence of uniform Cu thin-film thickness during the optimum growth condition process are inferred by using the curvature-based Stoney formula, which is gaining increasingly widespread application in evaluating the stresses in a thin-film on a substrate. Furthermore, this chapter has focused on determining completely growth mechanism of the new phenomenon in the research, which can promote the growth of high-quality Cu_2O nanowires. A new growth mechanism based on stress-redistribution phenomenon has been proposed for describing the formation and growth of these hillocks and nanowires, and a creative Cu_2O nanowire growth condition is confirmed in support of theory.

Chapter 4 Nanowire Growth at Predetermined Positions

Recently, nanowires have quickly become the focus of intensive research owing to their unique properties. Besides their importance to fundamental understanding of properties and phenomena, nanowires play also an important role as numerous applications mentioned in previous chapters, including chemical sensors,[84] electronic devices and interconnects,[85, 86] and etch masks[87] and even more promising application fields. Patterning nanowires at predetermined positions can show great potential in nanoscale device fabrication and functional unit integration field, and also induce enhanced properties.

To the present day, many researchers have considered that the specific challenge is the simultaneous, parallel fabrication of large arrays of nanowires under precisely controlled positions with desired patterns for integration them into complex structures in nanoscale devices, which may find desired functionalities and more applications in much wider fields. In order to the purpose, it is highly beneficial to find a simple and cost-effective method from a technological and applicable point of view in the pursuit of next-generation high-performance nanoscale devices. So far, it still remains a significant challenge.

Integration of the high-quality copper oxide nanowires into useful nanoscale devices requires placing them in specific positions with desired patterns reproducibly. Copper

oxide nanowires fabricated by the stress-induced method are known to grow where the copper is deposited. By further exploiting this trait, nanowires can be grown in patterning regions of the substrate, by e-beam deposition of copper on the substrate surface.

Photolithography technique is an optical means for transferring patterns from mask onto a substrate surface. It is the primary method used to pattern devices and has played a key role as the microelectronics evolves.

In this chapter, combining the advanced photolithography technique, which is attractive for inexpensive and simple feature, can not only make sure patterning growth of aligned copper oxide nanowires from multilayer thin-film substrates for various applications, such as nano-optoelectronic, nanosensor, and nanogenerator applications, but also realize the need for systematic incorporation into more sophisticated and larger nanoscale device architectures.

4.1 Photolithography Process

Standard photolithography, using a mask, is often used for patterning purpose. A beam of light (typically ultraviolet light) passes through the mask and a lens, which focuses an image on photoresist (photosensitive coating of organic polymer) placed on a surface of a silicon wafer or a film. The parts that are exposed to the photoresist can be removed to leave the desired patterns on the silicon wafer or film. The resolution of the photolithography process determines the width of the channels. In photolithography, one

typically uses mask in which the desired patterns are defined as perfectly opaque and transparent regions.

The mask is designed with many different diameter columns in the research, shown in Figure 4.1.

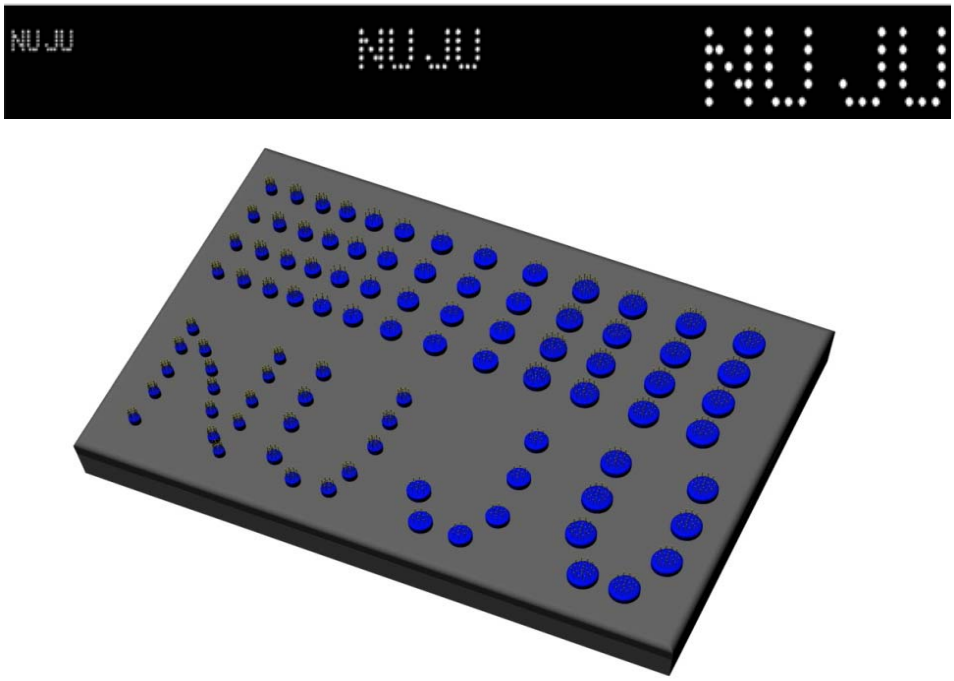

Figure 4.1 Schematic two and three-dimensional diagrams of the mask.

Photolithography is the process of transferring geometric shapes on a mask to the substrate surface covered with a photosensitive polymer in a very efficient way. Photolithography, employed in industry for mass production, can usually fabricate structures as small as 0.2 μm.

Prior to use, the substrates are firstly rinsed using acetone and isopropyl alcohol for 5 minutes with ultrasonics. A clean substrate surface free from dust, photoresist residue,

and from other material sources is required for a successful pattering with photolithography. Then, the substrate is baked in an oven at 200℃ for 30 minutes to remove all moisture.

To start the photolithographic process, a layer of UV (ultraviolet light)-sensitive photoresist is deposited on the substrate surface. By spin-coating, a homogeneous thickness and distribution of the photoresist on the whole substrate surface is achieved. The OAP film as sensitive photoresist is spun to coat on the substrate surface at 3000 rpm for 20 seconds, and then the substrate is baked at 90℃ for 1 minute. Another photoresist layer of AZ-5214E is spun to cover the substrate surface at 2000 rpm for 27 seconds, and the substrate is subsequently baked at 115℃ for 3 minutes. This baking step is used to evaporate the coating solvent, and densify the photoresist after spin-coating.

After baking step, the substrate is brought in aligned contact with the mask and exposed to UV light for a specific time, which is determined by the type and thickness of photoresist. UV light is projected through the patterning mask resulting in a whole pattern transfer onto the photoresist layer. In the experiment, the exposure time is 3.3 seconds. The exposure to UV light alters the chemistry of the photoresist and changes its solubility relative to unexposed resist. There are two types of photoresist, namely “positive” and “negative”. When a positive photoresist is exposed to UV light, the energetic photons of the light break certain bonds in the long-chain polymers of the photoresist, causing them to become shorter and thus more soluble. A developer easily washes away the exposed

areas, leaving behind a copy of the pattern on the mask. When a negative photoresist is exposed to UV light, it causes cross-linking between the photoresist polymers making the exposed areas less soluble. The developer removes the unexposed photoresist, leaving behind a negative image of the mask.

A negative photoresist is used in this research, and the typical photolithography process is shown in Figure 4.2.

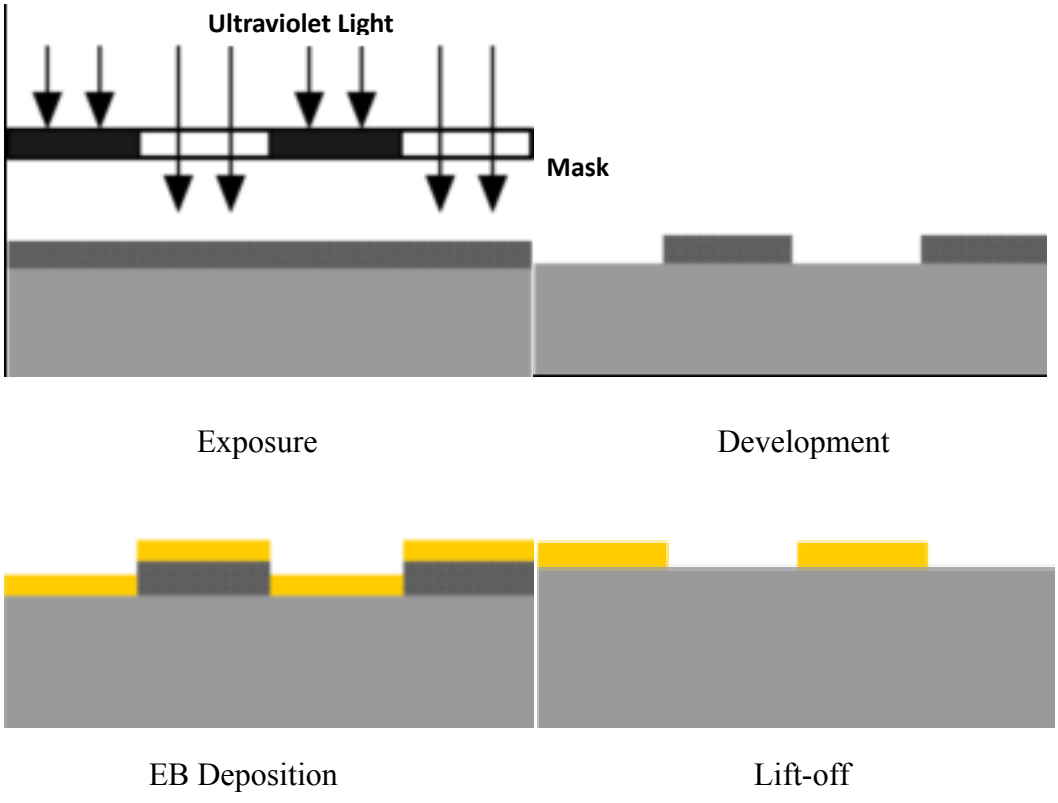

Figure 4.2 Schematic procedures for photolithography technique.

In the case of a negative photoresist, the goal is to transfer this pattern into the photoresist such that the photoresist is completely removed in the opaque regions and

completely remained in the transparent regions. As a result, the pattern is transferred into the photoresist as a gradual change in photoresist chemistry from soluble to insoluble, corresponding to the opaque- transparent transition in the mask.

After the exposure to UV light, the substrate is placed in developer to remove unexposed photoresist, then followed by a DI water rinse and a post-bake at 115 ℃ for 3 minutes. Some parts of the UV exposed substrate are protected under a layer of photoresist while other regions underneath substrate are exposed.

Then, 60 nm of Ta and 400 nm of copper are deposited onto the substrate by using EB deposition technique mentioned in the previous chapter 2.1. The metals are deposited on all over the substrate surface wherever the photoresist has been removed. After metal deposition, the substrate is then immersed into acetone with ultrasonics to remove the photoresist and the metal deposited on it, the unwanted Cu layer on the photoresist, and any other residues. The substrate is then cleaned using ID water.

After the lift-off process of stripping all unwanted Cu film, the designed patterning Cu layer of the mask is transferred to the substrate. The substrate is then cut into small pieces, and the experimental procedure of nanowire growth follows the steps also mentioned the previous chapter 2.1.

Here, some results from SEM observation are shown in Figure 4.3.

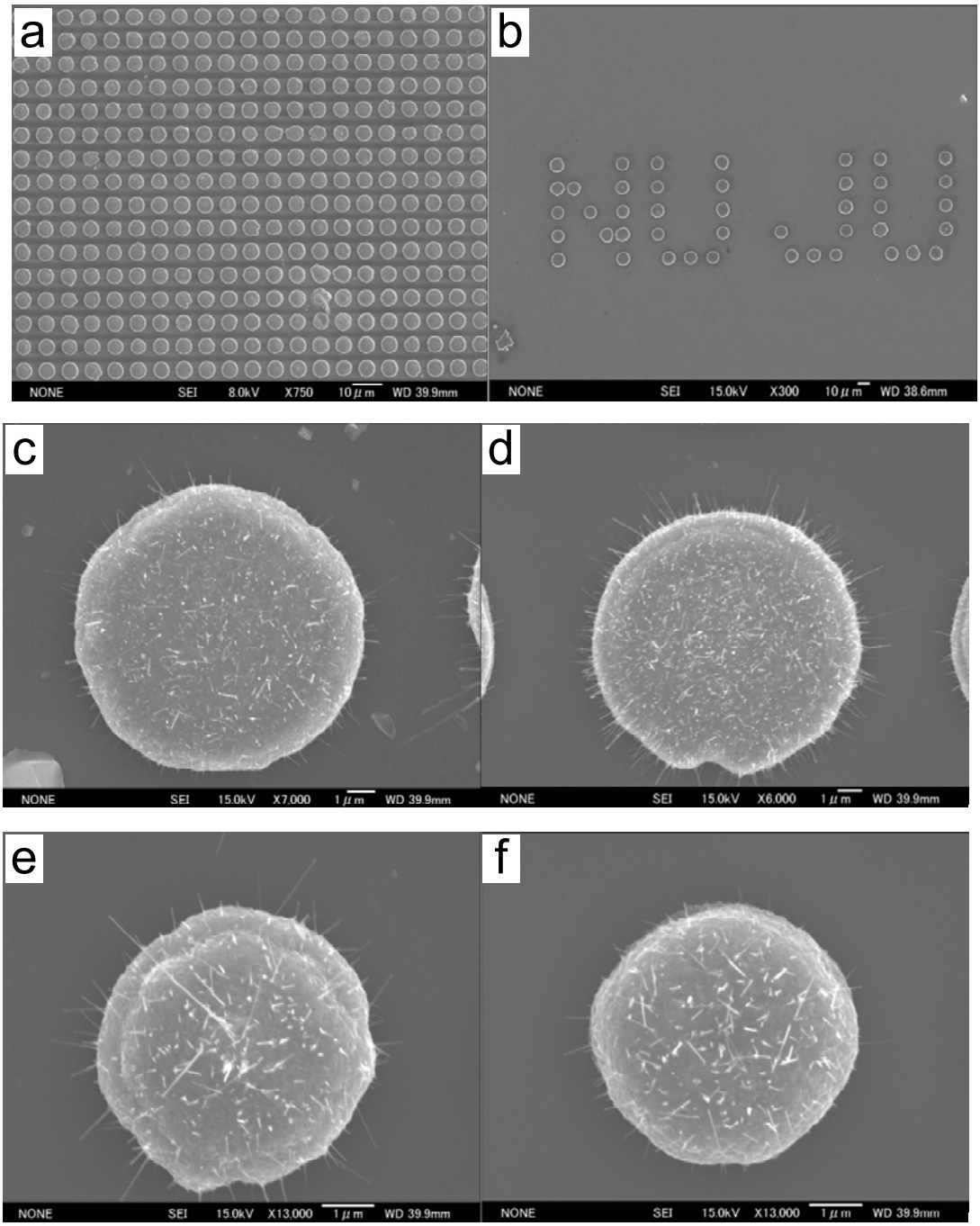

Figure 4.3 SEM images of patterns and nanowire growth on columns. (a) overall nanowire growth on columns, (b) nanowire growth on desired patterns, (c) and (d) nanowire growth on 10 μm column, (e) and (f) nanowire growth on 5 μm column.

From these SEM images, the nanowire growth on columns at predetermined positions is not so good. To our knowledge, many parameters can affect the nanowire growth under these conditions. After overall analysis, these results suggest that the amount of copper supply may be an important parameter for nanowire growth under the condition.

In order to obtain better nanowire growth, some measurements are adopted.

4.2 Improvement

To increase the amount of copper supply, a 400 nm Cu film is deposited on the substrate surface using EB deposition technique before the photolithography process at first, and then the procedure follows the above mentioned steps, as shown in Figure 4.4.

a Cu film deposition beforehand

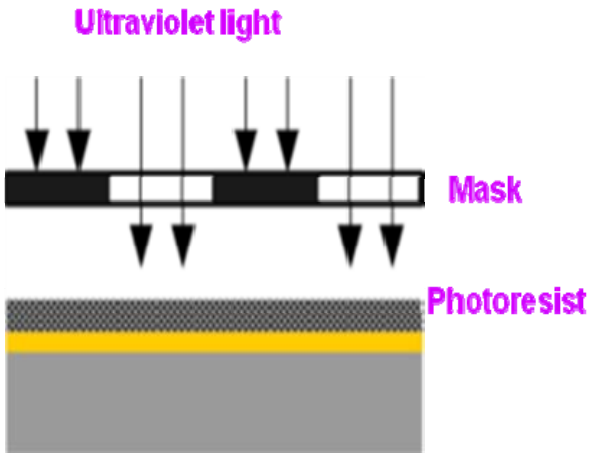

Exposure

Development

EB Deposition Lift-off

Figure 4.4 Schematic improved procedures for photolithography technique.

Here, another some results from SEM observation are shown in Figure 4.5.

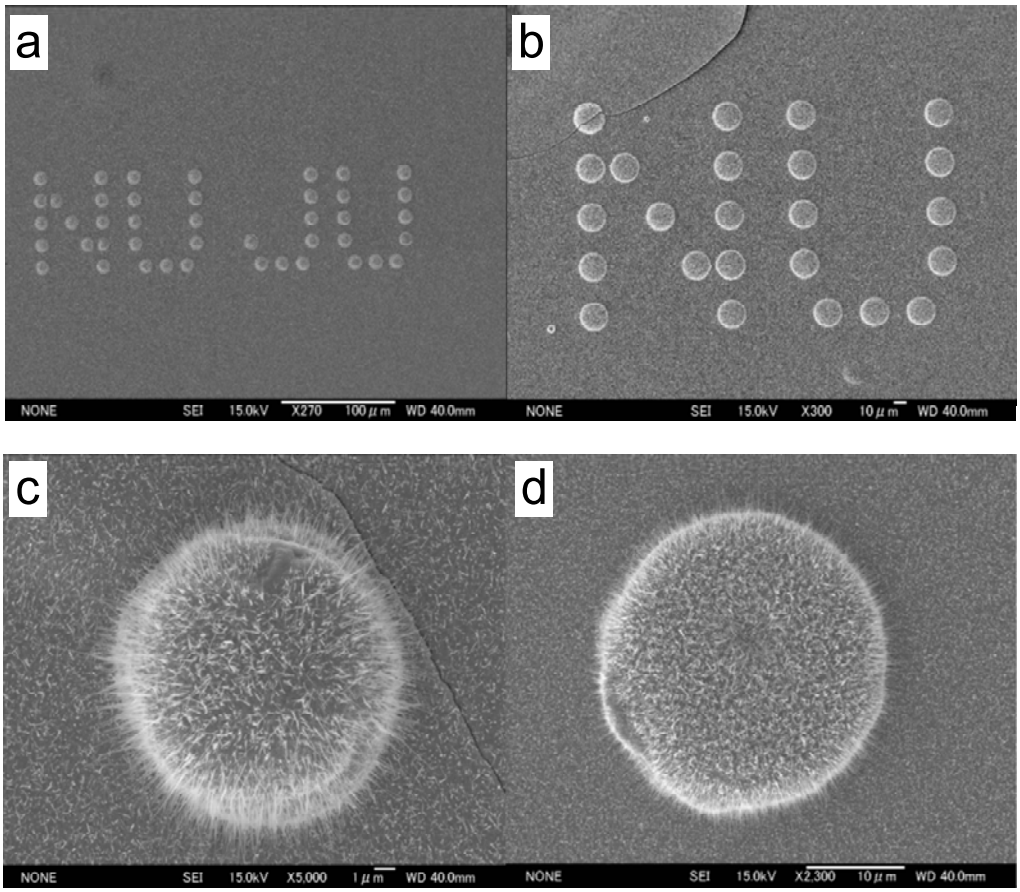

Figure 4.5 SEM images of patterns and nanowire growth on columns. (a) and (b) desired patterns for different magnification times, (c) nanowire growth on 10 μm column, (d) nanowire growth on 20 μm column.

From these SEM images, obviously, the nanowire growth on columns at predetermined positions is much better than the above results, shown in Figure 4.3. Uniform nanowires with high density grow from the patterning Cu thin film.

The amount of copper supply can greatly affect nanowire growth on defined patterns at predetermined positions.

In summary, the position-controlled patterning copper oxide nanowire growth is achieved by the combination of photolithography technique, which opens up many possibilities in futuristic nanoscale device applications. The low-cost process has a great potential for scale-up, mass production and a diversity of commercial applications once the defects of as-obtained copper oxide nanowires can be reduced to a device-function tolerable level.

Although the work is still in blueprint or initiation stage, the technique presents successful examples of patterning copper oxide nanowire growth in selected positions as promising targets of future research.

Chapter 5 Photovoltaic Application

As inspired by distinct mechanic, electronic, optical, chemical and physical properties of one-dimensional nanostructures, their application research is expanding rapidly into the forefront research in nanotechnology. Many different applications have been realized based on one-dimensional nanostructures, such as field-effect transistors,[88] ultra-sensitive nanometer-size gas sensors[89] and humidity sensors,[90] nanoresonators,[91] nanocantilever,[92] and nanogenerators.[93, 94, 95]

Harvesting energy directly from sunlight using photovoltaic technology is being increasingly recognized as an essential component of future global energy production. Solar energy production is fast becoming a vital source of renewable energy being developed as an alternative to traditional fossil fuel-based sources of power. Solar cells based on the semiconductor nanostructures such as Si and ZnO nanowires or nanorods have been reported in recent years.[96, 97, 98, 99, 100] The broad exploratory development is largely triggered by the finding that nano-structuring can markedly improve the electronic transport in solar cells. The p-n junctions in the aforementioned works have been fabricated by depositing other materials onto the semiconductor nanowire or nanorod arrays to form the multi-layer structure.[98, 99] or core-shell structure.[100] One of the primary challenges to the full-scale implementation of solar energy remains the expensive cost associated with the construction of photovoltaic modules and certain toxic elements in

some thin film solar cells. This unfavorable cost has so far prohibited the technology from having a significant impact on global energy production. The principal photovoltaic (PV) material on the market today is silicon. Although silicon-based solar cells are comprised of a very abundant element, their large-scale production is hampered by the high cost of processing and refining, which sets the average electricity cost from a silicon solar cell well above that which comes from coal- or gas-burning power plants.[101, 102]

If a material is truly to become a marketable option for the photovoltaic industry, some consideration must be given to the expense of its synthesis, manufacture, processing, and construction into a device, in addition to its ultimate PV efficiency. Generally speaking, materials selection for future photovoltaics should satisfy several important criteria. First, the materials should be comprised of abundant and inexpensive elements. Second, the materials should be environmentally benign to avoid any issues of potential environmental contamination. Last, importantly for any potential PV application, the materials must have an optimal band gap to maximize solar absorption such that the resulting solar cell would have marketable energy conversion efficiency.

Among all materials proposed as a PV alternative to silicon, cuprous oxide (Cu_2O) is one of the most extensively studied[103] with investigations stretching back more than 20 years. The semiconducting material is doped with specific dopants to create the required p-type or n-type semiconductor. A semiconductor doped with donor atoms is known as an n-type semiconductor as the charge carriers are electron, which have a negative charge.

A semiconductor doped with acceptor atoms is known as a p-type semiconductor as the charge carriers are holes, which have an effective positive charge. Cu_2O is a natural p-type semiconductor with a direct energy gap of 2.1 eV.[17, 104] Such large exciton energy can ensure an efficient exciton emission at room temperature under low excitation energy, which allows for good solar spectral absorption. It is also a technologically important and promising material for photovoltaic applications because the theoretical energy conversion efficiency of a Cu_2O solar cell has been predicted to be around 20%.[105, 106]

Moreover, Cu_2O is cheap and plentiful with low toxicity and good environmental acceptability, and can be readily prepared as large-area samples.[107] The abundance and nontoxicity allow for the possibility of constructing durable, long-lasting solar cells with Cu_2O as the active light-absorbing component. There are several examples of Cu_2O-based PV devices reported in the literature, often prepared by using solution-based methods.[19, 108, 109, 110] However, nearly all of these devices are either bulk or thin-film bilayer structures, and these types of structures suffer from the fact that the optimal material length scales for optical absorption and carrier extraction are contrary to one another. A thicker film can absorb more sunlight, but only the excitons created near the active interface can also be effectively split and harvested into an external circuit. So far, although Cu_2O-based solar cells have been extensively investigated, there are no reports of any exhibiting an energy conversion efficiency over 1%.[105, 111, 112, 113]

Nanowire-based solar cells have been reported to possess inherent advantages over

traditional bilayer devices,[96, 114, 115, 116, 117] including lower production costs and using much less material. However, relatively little work has focused on the implementation of nanowire-based structures in inexpensive, stable solar cell.

In the research, a thin Cu_2O layer forms naturally during the heating process in the air, and the structure with arrays of Cu_2O nanowires coated by Cu_2O layer can be obtained immediately after the growth of nanowires. The contact between metal (Cu) and a semiconductor surface (Cu_2O) is known as a Schottky barrier. Therefore, after contact, electrons will flow from the metal (Cu) to the semiconductor (Cu_2O). This causes a build-up of charges on both sides of the interface, resulting in an electrical field and a potential gradient, the so-called band bending. Finally, at the interface, in the so-called depletion region, there is a surplus of negative charge or uncompensated charge acceptors. The Schottky barrier forming on the Cu_2O/Cu interface can play a similar role as the p-n junction to generate the photovoltaic effect in the solar cells.[118, 119, 120] Therefore, it indicates a more convenient and simpler way to fabricate the potential solar cell based on as-obtained Cu_2O nanowire presented in this research. Besides, the large surface area to volume ratio of as-obtained nanowires, which indicates enhanced light absorption, may enhance the optical absorption performance. The improvement may also promise a good future for the solar cell. The fabricated Cu_2O nanowires have been proven to be defect-free and single-crystal ones with high aspect ratios, and they are of great potential for the devices in micro- and nano-optoelectronics.

In addition, to further verify the composition of the as-obtained nanowires, the photovoltaic effect of the multilayer sample with nanowires to solar cell is put forward to investigate.

5.1 Introduction

The basic idea of a solar cell is to convert light energy into electrical energy. The energy of light is transmitted by photons, small packets or quantum of light. Electrical energy is stored in electromagnetic fields, which in turn can make a current of electrons flow. Thus a solar cell converts light, a flow of photons, to electric current, a flow of electrons.

When photons are absorbed by matter in the solar cell, their energy excites electrons higher energy states where the electrons can move more freely. The perhaps most well-known example of this is the photoelectric effect, where photons give electrons in a metal enough energy to escape the surface. In an ordinary material, if the electrons are not given enough energy to escape, they would soon relax back to their ground states. In a solar cell, however, the way it is put together prevents this from happening. The electrons are instead forced to one side of the solar cell, where the build-up of negative charge makes a current flow through an external circuit. The current ends up at the other side (or terminal) of the solar cell, where the electrons once again enter the ground state, as they have lost energy in the external circuit.

In a word, a solar cell consists of a light absorbing material which is connected to an

external circuit in an asymmetric manner. Charge carriers are generated in the material by the absorption of photons of light, and are driven towards one or other of the contacts by the built-in spatial asymmetry. This light driven charge separation establishes a photovoltage at open circuit, and generates a photocurrent at short circuit. When a load is connected to the external circuit, the solar cell produces both current and voltage and can do electrical work.

Here, Schottky barrier is further introduced in detail. A Schottky barrier, named after Walter H. Schottky, is a potential barrier formed at a metal–semiconductor junction which has rectifying characteristics, suitable for use as a diode. The largest differences between a Schottky barrier and a p-n junction are its typically lower junction voltage, and decreased (almost nonexistent) depletion width in the metal. Not all metal–semiconductor junctions form Schottky barriers. A metal–semiconductor junction that does not rectify current is called an ohmic contact. Rectifying properties depend on the metal's work function, the band gap of the intrinsic semiconductor, the type and concentration of dopants in the semiconductor, and other factors. Design of semiconductor devices requires familiarity with the Schottky effect to ensure Schottky barriers are not created accidentally where an ohmic connection is desired.

Schottky barriers, with their lower junction voltage, find application where a device better approximating an ideal diode is desired. They are also used in conjunction with normal diodes and transistors, where their lower junction voltage is used for circuit

protection (among other things). Because one of the materials in a Schottky diode is a metal, lower resistance devices are often possible. In addition, the fact that only one type of dopant is needed may greatly simplify fabrication. And because of their majority carrier conduction mechanism, Schottky diodes can achieve greater switching speeds than p-n junction diodes, making them appropriate to rectify high frequency signals.

The most important difference between the p-n and Schottky diode is reverse recovery time, when the diode switches from non-conducting to conducting state and vice versa. Where in a p-n diode the reverse recovery time can be in the order of hundreds of nanoseconds and less than 100 ns for fast diodes, Schottky diodes do not have a recovery time, as there is nothing to recover from (i.e. no charge carrier depletion region at the junction). The switching time is ~100 ps for the small signal diodes, and up to tens of nanoseconds for special high-capacity power diodes. With p-n junction switching, there is also a reverse recovery current, which in high-power semiconductors brings increased EMI noise.

It is often said that the Schottky diode is a "majority carrier" semiconductor device. This means that if the semiconductor body is doped n-type, only the n-type carriers (mobile electrons) play a significant role in normal operation of the device. The majority carriers are quickly injected into the conduction band of the metal contact on the other side of the diode to become free moving electrons. Therefore no slow, random recombination of n- and p- type carriers is involved, so that this diode can cease

conduction faster than an ordinary p-n rectifier diode. This property in turn allows a smaller device area, which also makes for a faster transition. This is another reason why Schottky diodes are useful in switch-mode power converters; the high speed of the diode means that the circuit can operate at frequencies in the range 200 kHz to 2 MHz, allowing the use of small inductors and capacitors with greater efficiency than would be possible with other diode types. Small-area Schottky diodes are the heart of RF detectors and mixers, which often operate up to 50 GHz.

5.2 Sample Preparation

The samples for the photovoltaic effect investigation were prepared as follows, shown in Figure 5.1. First, a wire was connected to the top surface of the Cu/Ta/SiO_2/Si system by the high-temperature conductive adhesive (Pyro-Duct 597A, Oludec Ltd.), immediately after the EB evaporation process. Then the sample endured a heating and gradual cooling treatment as mentioned in the experimental procedure, chapter 2.1, and the Cu_2O/Cu multilayer structure with hillocks and Cu_2O nanowires was formed. Another wire was then connected to the surface of the Cu_2O layer by the same high-temperature conductive adhesive.

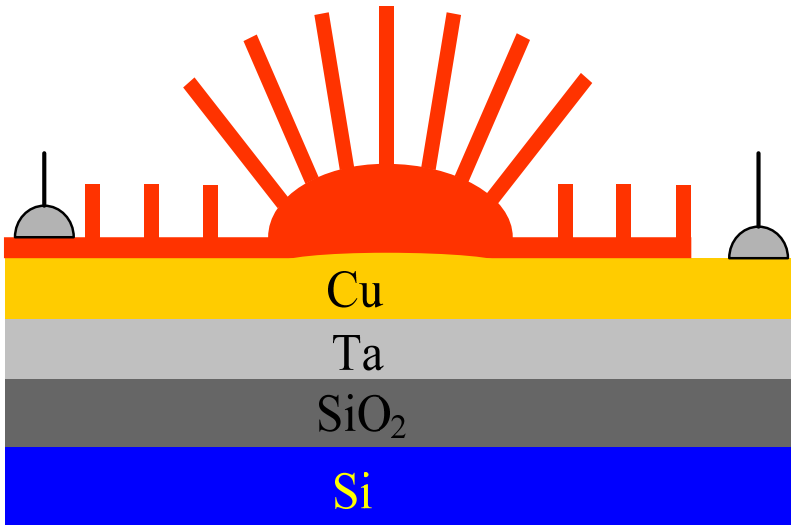

Figure 5.1 Schematic sample.

5.3 Dark Current Measurement

Studying the electrical characteristics of solar cells under dark conditions allows one to determine the device parameters and to predict the performance of the solar cell prior to deployment. The parameters derived from the dark current–voltage (*I–V*) characteristics can provide essential insights into the performance parameters which determine the efficiency of the device.

When a load is present, a potential difference develops between the terminals of solar cell. This potential difference generates a current which acts in the opposite direction to the photocurrent, and the net current is reduced from its short circuit value. This reverse current is usually called the dark current in analogy with the current I_{dark} (V) which flows across the device under an applied voltage, or bias, V in the dark. Most solar cells behave

like a diode in the dark, admitting a much larger current under forward bias ($V > 0$) than under reverse bias ($V < 0$). This rectifying behavior is a feature of photovoltaic devices, since an asymmetric junction is needed to achieve charge separation. The parameters extracted from the dark *I–V* curve of the solar cells are series resistance, shunt resistance, saturation currents and ideality factors. The dark current is roughly proportional to the area of the solar cell, the dark current density, $J = I/A$, is often used to compare solar cells.

To obtain the dark current curve, the measurement circuit was connected, as shown in Figure 5.2 (a), and the dark current curve is shown in Figure 5.2 (b). The rectifying behavior in the dark current curve indicates that a Schottky barrier is formed on the Cu_2O/Cu interface.

With +100 mV applied bias, it is found that the forward current density of this sample is 0.56 mA/cm^2, while the reverse leakage current density is 0.023 mA/cm^2 when -100 mV is applied

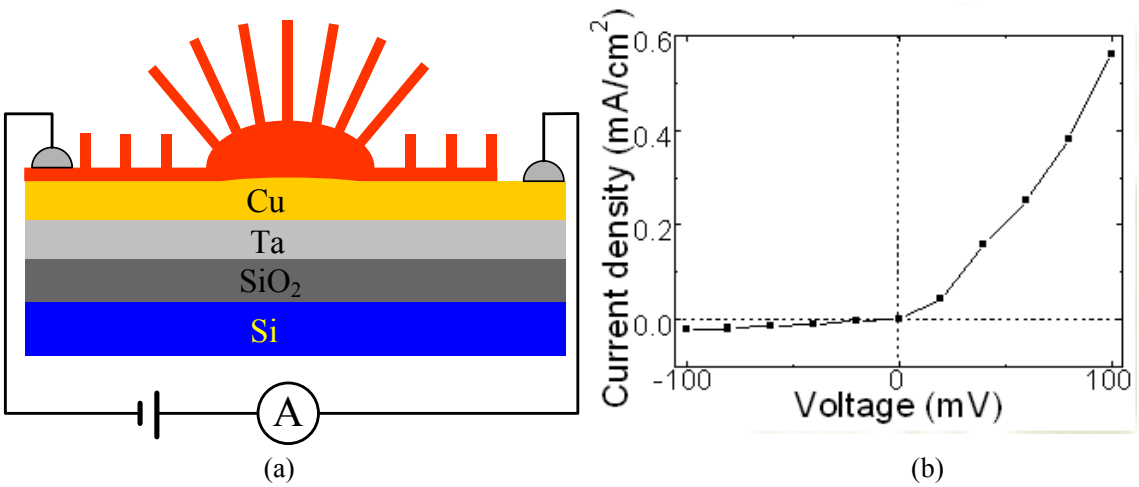

(a) (b)

Figure 5.2 (a) Schematic measurement sample, and (b) dark current curve.

5.4 Photovoltaic Current Density-Voltage (*J-V*) Curve

The *J-V* characteristic when referring to current density, also known as the Current Voltage (*I-V*) characteristic, is a commonly used tool for analyzing the electrical characteristics of the photovoltaic devices. *J-V* characteristics simply show the current flows through a device as the voltage applied to it is varied. *J-V* characteristics for solar cells exposed to a light source are often recorded using a continuous light source. This is, the light source remains the whole process while the current density and voltage measurements are taken.

Information such as resistance and conductance can be gleaned using this technique. In the case of semiconductor, the conductance can be measured for different regions of the *J-V* curve. The resistance is simply the inverse of the conductance. Photoconductivity can be observed by exposing the simple to a light source while the *J-V* characteristic is being

measured. This technique is often used to analyze the performance of solar cells. It gives information on the basic electrical properties of a solar cell including the fill factor (*FF*), short circuit current density (J_{sc}) and open circuit voltage (V_{oc}), from which other factors such as the energy conversion efficiency (η) of the solar cell can be calculate. The short circuit current density (J_{sc}) is defined as the output current density under illumination where the bias voltage, or the voltage applied to the sample, is zero. The open circuit voltage (V_{oc}) is defined as the bias voltage under illumination where the output current density is zero. The maximum voltage (V_{max}) and maximum current density (J_{max}) are found from the maximum power point, the point on the *J*-*V* curve for the illuminated cell where the product of *V* and *J* is greatest. From this information the energy conversion efficiency (η) and fill factor (*FF*) can be found.

Energy conversion efficiency (η) is the essential parameter for solar cells with respect to maximizing energy production and minimizing cost. Low energy conversion efficiency demands a larger photovoltaic active area in order to produce the same energy output.

The cell efficiency (η) is defined as:

$$\eta = \frac{P_{out}}{P_{in}} \qquad (5\text{-}1)$$

and can be found from:

$$\eta = \frac{J_{max} V_{max}}{P} \qquad (5\text{-}2)$$

where P_{out} is the power output from the solar cell, P_{in} is the power incident upon the solar cell from the source of illumination, and *P* is the power incident upon the solar cell per

unit area.

The fill factor (*FF*) is defined as:

$$FF = \frac{J_{max} \square V_{max}}{J_{sc} V_{oc}} \qquad (5\text{-}3)$$

The quantum efficiency of a solar cell is the percentage of incoming photons that are converted to outgoing current. The fill factor (*FF*) is an indication of the quality of the solar cell. The higher the fill factor the closer to the ideal square *J-V* characteristic. The fill factor is a measure of the extent to which the *J-V* curve fills the power quadrant.

To obtain the photovoltaic current density-voltage (*J-V*) curve of the solar cell sample, the measurement circuit has been connected shown in Figure 5.3 (a), and typical solar cell behavior can be observed in the photovoltaic current density-voltage (*J-V*) curve as shown in Figure 5.3 (b). From the curve, the shape of the *J-V* curve is similar with that of the Cu_2O/n-ZnO nanowire solar cell.[98]

The sample is illuminated by a lamp (SPH-50, Takada Ltd.), the light of which is focused within a small area about 2 mm^2. The light power of the lamp is measured to be 443 μW. Solar cell parameters, such as open circuit voltage (V_{oc}) and short circuit current density (J_{sc}), can be read from the photovoltaic *J-V* curve shown in Figure 5.3 (b) to be 7.5mV and 2.67 $\mu A/cm^2$, respectively. The fill factor (*FF*) and efficiency (η) can also be calculated from the J-V curve.

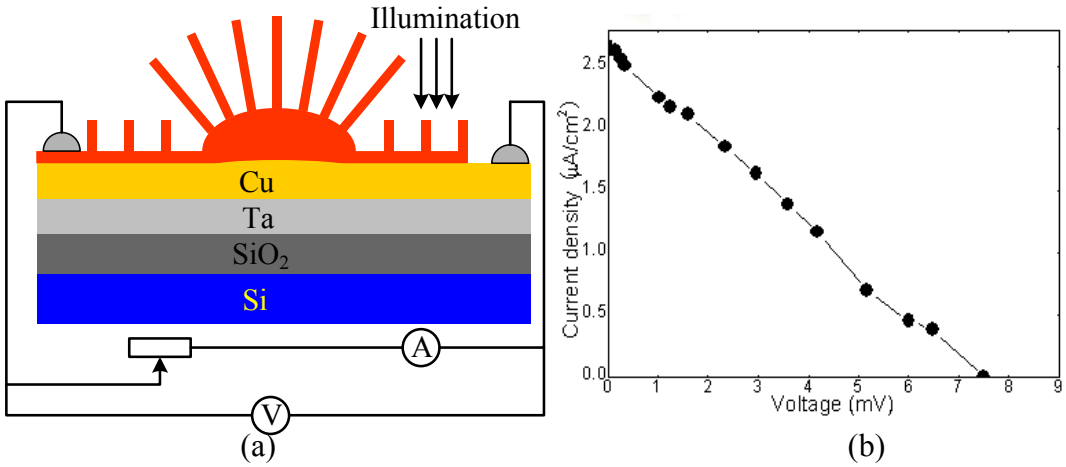

Figure 5.3 (a) Schematic solar cell sample, and (b) photovoltaic current density-voltage (J-V) curve.

However, the photovoltaic current density and voltage of the present solar cell sample are relatively low. The fill factor (*FF*) is 0. 25, namely $FF = (J \times V)_{max} / (J_{sc} \times V_{oc}) \approx 0.25$. And its energy conversion efficiency (η) is only about 2.26×10^{-5} %.

The typical photovoltaic effect further demonstrates that the main composition of the nanowires and the sample surface is Cu_2O rather than Cu or CuO.

It can be also observed that, when the focused light scanned on the sample surface from one point to the others, the photovoltaic voltages are quite different. The area with more hillocks and well-grown Cu_2O nanowires always corresponds to higher photovoltaic voltage. The sample (without hillocks and well-grown nanowires) under natural cooling process and the sample heated at a relatively low temperature (without nanowires) are also studied, but no obvious solar cell effect can be observed. Therefore, the observed photovoltaic effect of the sample is mainly contributed by the well-grown

Cu_2O nanowires.

It should be mentioned that the observed photovoltaic current density and voltage of the present sample are relatively low, and the energy conversion efficiency remains far below theoretical expectations.

The main cause of the low energy conversion efficiency of Cu_2O nanowire solar cell sample at the present stage is the presence of microcracks on the sample surface after the heating and gradual cooling process in particular, which may bring up the inner resistance of the sample and lead to smaller photovoltaic current. Besides, the low energy conversion efficiency appears to be also dominated by multiple-step process, presumably because of dislocations and impurities in the Cu_2O samples.

To produce more efficient Cu_2O nanowire solar cell, the method proposed in this research should be further improved to reduce the microcracks on the sample surface, and to generate more hillocks with well-grown Cu_2O nanowires. Cu_2O nanowire arrays offering a larger surface area here provide feasibility to the enhanced photoelectric energy conversion efficiency. Much effort is still needed to increase the energy conversion efficiency of Cu_2O nanowire solar cell. Clearly, a thorough understanding and remedy for all the above-mentioned problems demand more basic and applied investigation of the procedure. It is firmly believed that there is still enough room for further improving the energy conversion efficiency in near future.

In summary, the typical photovoltaic effect has been demonstrated to exist in this

Cu_2O/Cu multilayer structure with the high-quality Cu_2O nanowire arrays, which makes it a potential option for cheap and low toxicity solar cells with good environmental acceptability. The stress-induced method with simplicity, low-cost, and template-free, which has successfully been used to fabricate Cu_2O nanowires, provides potential for large-scale solar cell production.

Although it is still in its infancy and the performance remains very poor, the Cu_2O/Cu multilayer structure with higher absorbance of light thus fabricated sheds light on developing better Cu_2O nanowire-based nano-optoelectronic devices and solar cells.

Chapter 6 Conclusions

6.1 Conclusions

Owing to the creation and discovery of novel nanostructures that provide interesting and functional targets for scientific studies, and the establishing of new theories that predict and explain the new or improved phenomena in nanometer scale, nanotechnology is experiencing a flourishing development in a large variety of fields covering all of the areas from science to engineering and to biology.

As an active field in nanotechnology, the work presented in this dissertation is mostly focused on the fundamental study about the fabrication, growth mechanism and application of Cu_2O nanowires.

Here, a creative stress-induced method for growing high-quality single-crystalline Cu_2O nanowires is presented. For the first time, the gradual cooling process is emphasized and exhibits significant effects on nanowire growth and nanowire composition in detail. Therefore, a systematic research has been conducted to optimize the growth condition for achieving Cu_2O nanowires. The high-quality Cu_2O nanowires with larger aspect ratio and higher growth density have been derived under the optimum growth condition of cooling gradually for 4 hours after heating for 5 hours. This method also provides a much simpler way to fabricate reproducibly Cu_2O nanowires at low cost and at large quantity.

This dissertation is also to set about the study of the relationship between nanowire diameter and thin copper film thickness. It has been found that the diameter of Cu_2O nanowires varies according to the thickness of copper thin film. Generally, thinner copper thin film results in smaller nanowire diameter. This could be an effective and simple path to control nanowire diameter. It is believed that the ability to control over the diameter and aspect ratio of Cu_2O nanowires will facilitate the study of their fundamental properties and the exploration of their new future applications in electronic, optical and optoelectronic nano-devices and sensors. Moreover, the discoveries provide a road map for large-scale, controlled fabrication of Cu_2O nanowires with the potential to meet the needs of practical applications and commercialization, and also open to a new way to manipulate nanomaterials.

The growth mechanism also is deeply analyzed to better understand the film stress effects in the dissertation. A new stress-redistribution theory related to the gradual cooling process has been set up.

In addition, patterning copper oxide nanowire growth at predetermined positions through the low-cost photolithography technique has also been successfully achieved, which indicates a revolutionary science and technology. More applications should be developed by using as-obtained copper oxide nanowires in new generation nano-device fabrication and integration.

The typical photovoltaic effect is demonstrated to exist in this Cu_2O/Cu multilayer

structure with Cu_2O nanowire array, which makes it a potential option for cheap and low toxicity photovoltaic devices with good environmental acceptability. Although the overall conversion efficiency of Cu_2O nanowire solar cells is not optimized yet, the research paves the way for a simple and economic approach to fabricating these novel photovoltaic devices.

Due to the low cost and high efficiency, the techniques may eventually become the dominant fabrication method in future nanotechnology. With the improvement of the present stress-induced method demonstrated in this dissertation, it is believed that the approach can be extended to other material types of film grown nanowires, and thus could open up exciting opportunities for fundamental studies and technological applications of a wide-range of nanomaterials in the future. In addition, the availability of high-quality Cu_2O nanowires should be able to bring in new types of applications or enhance the performance of currently existing devices as a result of quantum-size effects.

In brief, the work presented in this dissertation may set a firm foundation for many industrial applications from controlled fabrication to nanomanufacturing. The method, avoiding complicated processes and special instruments, can be extended as a general method to prepare other metal oxide nanowires.

6.2 Recommendations for Future Work

The following further work is recommended as a result of this research.

1) The stress-induced method with emphasized gradual cooling process should be developed to fabricate other material high-quality nanowires, and explore their much more advanced applications.
2) Further analyses of Cu_2O nanowire growth and the operating factors, such as temperature, heating time, and nuclei distribution, and so on, should be investigated.
3) More studies are necessary to understand the nanowire growth mechanism in depth in order to precisely control nanowire growth for special applications.
4) Effective methods should be adopted to increase the performance of Cu_2O nanowire-based photovoltaic devices.
5) Fabrication of high-quality desired nanowires at designated locations is urgent and attractive, and their unique various kinds of applications should also be explored for next-generation complicated nanodevices.

REFERENCES

1. H. Morkoc, S. Strite, G. B. Gao, M. E. Lin, B. Sverdlov, and M. Burns, *J. Appl. Phys.* 1994, 76 (3): 1363-1398.

2. A. V. Krishnamoorthy and K. W. Goossen, *IEEE J. Sel. Top. Quant.* 1998*,* 4 (6): 899-912.

3. J. Janata, *Anal. Chem.* 1992, 64 (12): R196-R219.

4. A. P. Alivisatos, A. L. Harris, N. J. Levinos, M. L. Steigerwald, and L. E. Brus, *J. Chem. Phys.* 1988, 89 (7): 4001-4011.

5. P. Buffat, and J. P. Borel, *Phys. Rev. A* 1976, 13 (6): 2287-2298.

6. S. Iijima, *Nature* 1991, 354 (6348): 56-58.

7. Z. L. Wang, "Nanowires and Nanobelts: Materials, Properties and Devices", *Kluwer Academic Publishers*, Boston (2003).

8. Y. N. Xia, P. Yang, Y. Sun, Y. Wu, B. Mayers, B. Gates, Y. Yin, F. Kim, H. Yan, *Adv. Mater.* 2003, 15 (5): 353-389.

9. X. F. Duan, Y. Huang, Y. Cui, J. F. Wang, C. M. Licber, *Nature* 2001, 409 (6816): 66-69.

10. S. J. Hurst, E. K. Payne, L. Qin, C. A. Mirkin, *Angew. Chem. Int. Edit.* 2006, 45 (17): 2672-2692.

11. S. R. Nicewarner-Pena, R. G. Freeman, B. D. Reiss, L. He, D. J. Pena, I. D. Walton,

R. Cromer, C. D. Keating, M. J. Natan, *Science* 2001, 294 (5540): 137141.

12. A. M. Morales, C. M. Lieber, *Science* 1998, 279 (5348): 208-211.

13. C. M. Lieber, *MRS Bull.* 2003, 28 (07): 486-491.

14. W. Liu, C. M. Lieber, *J. Phys. D: Appl. Phys.* 2006, 39 (14): R387–R406.

15. Y. Li, F. Qian, J. Xiang, C.M. Lieber, *Mater. Today* 2006, 9 (10): 18-27.

16. C. Thelander, P. Agarwal, *Mater. Today* 2006, 9 (10): 28-35.

17. R. N. Briskman, *Sol. Energy Mater. Sol. Cells* 1992, 27 (4): 361-368.

18. Z. Z. Chen, E. W. Shi, Y. Zheng, W. J. Li, B. Xiao, J. Y. Zhuang, *J. Cryst. Growth* 2003, 249 (1-2): 294-300.

19. K. Akimoto, S. Ishizuka, M. Yanagita, Y. Nawa, G. K. Paul, T. Sakurai, *Solar Energy* 2006, 80 (6): 715-722.

20. T. Mahalingam, J. S. P. Chitra, J. P. Chu, H. Moon, H. J. Kwon, Y. D. Kim, *J. Mater. Sci. -Mater. Electron.* 2006, 17 (7): 519-523.

21. A. Mittiga, E. Salza, F. Sarto, M. Tucci, R. Vasanthi, *Appl. Phys. Lett.* 2006, 88 (16): 163502.

22. C. M. McShane, K. S. Choi, *J. Am. Chem. Soc.* 2009,131 (7): 2561-2569.

23. J. Zhang, J. Liu, Q. Peng, X. Wang, Y. Li, *Chem. Mater.* 2006, 18 (4): 867-871.

24. H. Zhang, Q. Zhu, Y. Zhang, Y. Wang, L. Zhao, B. Yu, *AdV. Funct. Mater.* 2007, 17 (15): 2766-2771.

25. B. White, M. Yin, A. Hall, D. Le, S. Stolbov, T. Rahman, N. Turro, S. O'Brien, *Nano*

Lett. 2006, 6 (9): 2095-2098.

26. H. Yu, J. Yu, S. Liu, S. Mann, *Chem. Mater.* 2007, 19 (17): 4327-4334.

27. P. Poizot, S. Laruelle, S. Grugeon, L. Dupont, J. M. Taracon, *Nature* 2000, 407 (6803): 496 -499.

28. J. N. Nian, C. C. Hu, H.Teng, *Int. J. Hydrogen Energy* 2008, 33 (12): 2897-2903.

29. Y. Y. Wu, T. Livneh, Y. X. Zhang, G. S. Cheng, J. F. Wang, J. Tang, M. Moskovits, Galen D. Stucky, *Nano Lett.* 2004, 4 (12): 2337-2342.

30. A. L. Daltin, A. Addad, J. P. Chopart, *J. Cryst. Growth* 2005, 282 (3-4): 414-420.

31. R. Inguanta, S. Piazza, C. Sunseri, *Electrochim. Acta.* 2008, 53 (22): 6504-6512.

32. H. S. Shin, J. Y. Song, J. Yu, *Mater. Lett.* 2009, 63 (3-4): 397-399.

33. X. Hong, G. Z. Wang, W. Zhu, X. S. Shen, Y. Wang, *J. Phys. Chem. C* 2009, 113 (32): 14172-14175.

34. Y. Tan, X. Xue, Q. Peng, H. Zhao, T. Wang, Y. Li, *Nano Lett.* 2007, 7 (12): 3723-3728.

35. M. Z. Wei, N. Lun, X. C. Ma, S. L. Wen, *Mater. Lett.* 2007, 61 (11-12): 2147-2150.

36. S. Sahoo, S. Husale, B. Colwill, T. W. Lu, S. Nayak, Pulickel M. Ajayan, *ACS Nano* 2009, 3 (12): 3935-3944.

37. S. D. Watson, N. G. Wright, B. R. Horrocks, A. Houlton, *Langmuir* 2010, 26 (3): 2068-2075.

38. J. Y. Ji, P. H. Shih, C. C. Yang, T. S. Chan, Y. R. Ma, S. Y. Wu, *Nanotechnology*

2010, 21 (4): 045603.

39. Y. L. Qu, X. Y. Li, G. H. Chen, *Mater. Lett.* 2008, 62 (6-7): 886-888.

40. S. Wang, Q. Huang, X. Wen, X. Li, S. Yang, *Phys. Chem. Chem. Phys.* 2002, 4 (14): 3425-3429.

41. X. C. Jiang, T. Herricks, Y. N. Xia, *Nano Lett.* 2002, 2 (12): 1333-1338.

42. T. Yu, X. Zhao, Z. X. Shen, Y. H. Wu, W. H. Su, *J. Cryst. Growth* 2004, 268 (3-4): 590-595.

43. L. S. Huang, S. G. Yang, T. Li, B. X. Gu, Y. W. Du, Y. N. Lu, S. Z. Shi, *J. Cryst. Growth* 2004, 260 (1-2): 130-135.

44. A. Kumar, A. K. Srivastava, P. Tiwari, R.V. Nandedkar, *J. Phys.: Condens. Matter.* 2004, 16 (47): 8531-8543.

45. Y. W. Zhu, T. Yu, F. C. Cheong, X. J, Xu, C. T. Lim, V. B. C. Tan, J. T. L. Thong, C. H. Sow, *Nanotechnology* 2005, 16 (1): 88-92.

46. J. J. Chen, K. Wang, L. Hartman, W. L. Zhou, *J. Phys. Chem. C* 2008, 112 (41): 16017-16021.

47. B. Z. Lee, D. N. Lee, *Acta Mater.* 1998, 46 (10): 3701-3714.

48. S. M. Prokes, S. Arnold, *Appl. Phys. Lett.*2005, 86 (19): 193105.

49. M. Saka, F. Yamaya, H. Tohmyoh, *Scripta Mater.* 2007, 56 (12): 1031-1034.

50. Y. T. Cheng, A. M. Weiner, C. A. Wong, M. P. Balogh, M. J. Lukitsch, *Appl. Phys. Lett.* 2002, 81 (17): 3248-3250.

51. W. Shim, J. Ham, K. Lee, W. Y. Jeung, M. Johnson, W. Lee, *Nano Lett.* 2009, 9 (1): 18-22.

52. K. Hinode, Y. Homma, Y. Sasaki, *J. Vac. Sci. Technol.* 1996, 14 (4): 2570-2576.

53. D. Mijatovic, J. C. T. Eijkel, A. van den Berg, *LAB ON A CHIP* 2005, 5 (5): 492-500.

54. M. Alexe, C. Harnagea, D. Hesse, *J. Electroceram.* 2004, 12 (1-2): 69-88.

55. H. Ono, T. Nakano, T. Ohta, *Appl. Phys.Lett.* 1994, 64(12): 1511-1513.

56. H. J. Lee, K. W. Kwon, C. Ryu, R.Sinclair, *Acta Mater.* 1999, 47 (15-16): 3965-3975.

57. Y. Chang, M. L. Lye, H. C. Zeng, *Langmuir* 2005, 21 (9): 3746-3748.

58. Y. M. Yue, M. J. Chen, Y. Ju, L. Zhang, *Scripta Mater.* 2012, 66: 81-84.

59. S. K. Acharya, A. K. Rai, G. S. Kim, J. H. Hyung, B. G. Ahn, S. K. Lee, *Physica E* 2012, 44 (4): 839-842.

60. Y. Cui, L. J. Lauhon, M. S. Gudiksen, J. F. Wang, C. M. Lieber, *Appl. Phys. Lett.* 2001, 78(15): 2214-2216.

61. C. L. Cheung, A. Kurtz, H. Park, C. M. Lieber, *J. Phys. Chem. B* 2002, 106 (10): 2429-2433.

62. T. E. Bogart, S. Dey, K. K. Lew, S. E. Mohney, J. M. Redwing, *Adv. Mater.* 2005, 17 (1): 114-117.

63. N. Chopra, P. D. Kichambare, R. Andrews, B. J. Hinds, *Nano Lett.* 2002, 2 (10): 1177-1181.

64. Y. M. Yue, M. J. Chen, Y. Ju, *Nanosci. Nanotechnol. Lett.* 2012, Accepted.

65. L. E. Murr, "Electron and Ion Microanalysis, principles and Applications", *Marcel Dekker, Inc.* 2nd ed. New York (1991).

66. P. D. Yang, C. M. Lieber, *Science* 1996, 273 (5283): 1836-1840.

67. R. S. Wagner, W. C. Ellis, *Appl. Phys. Lett.* 1964, 4 (5): 89-90.

68. H. L. Cobb, "Camium Whiskers." *Monthly Review of the American Electroplaters Society*, 1946, 33: 28-30.

69. S. M. Arnold, S. E. Kounce, *J. Appl. Phys.* 1956, 27 (8), 964-966.

70. R. S. Wagner, W. C. Ellis, *Transactions of the Metallurgical Society of Aime* 1965, 233 (6): 1053-1055.

71. D. Wang, F. Qian, C. Yang, Z. H. Zhong, C. M. Lieber, *Nano Lett.* 2004, 4 (5): 871-874.

72. T. J. Trentler, K. M. Hickman, S. C. Goel, A. M. Viano, P. C. Gibbons, W. E. Buhro, *Science* 1995. 270 (5243): 1791-1794.

73. N. Wang, Y. F. Zhang, Y. H. Tang, C. S. Lee, S. T. Lee, *Appl. Phys. Lett.* 1998, 73(26): 3902-3904.

74. N. Wang, Y. H. Tang, Y. F. Zhang, C. S. Lee, S. T. Lee, *Phy. Rev. B* 1998, 58(24): 16024-16026.

75. S.M. Prokes, K. L. Wang, *Mrs Bulletin* 1999, 24 (8): 13-19.

76. T. I. Kamins, R. S. Williams, Y. Chen, Y. L. Chang, Y. A. Chang, *Appl. Phys. Lett.*

2000, 76(5): 562-564.

77. B. Mandl, J. Stangl, T. Martensson, A. Mikkelsen, J. Eriksson, L. S. Karlsson, G. Bauer, L. Samuelson, W. Seifert, *Nano Lett.* 2006, 6 (8): 1817-1821.

78. K. A. Dick, K. Deppert, T. Martensson, B. Mandl, L. Samuelson, W. Seifert, *Nano Lett.* 2005, 5 (4): 761-764.

79. Y. W. Wang, V. Schmidt, S. Stephan, *Nature Nanotechnology* 2006, 1 (3): 186-189.

80. G. G. Stoney, *Proc. R. Soc.* London, Ser. 1909, 82(553): 172-175.

81. M. Finot, S. Suresh, *J. Mech. Phys. Solids* 1996, 44 (5): 683-721.

82. A. Wikstrom, P. Gudmundson, S. Suresh. *J. Mech. Phys. Solids* 1999, 47 (5): 1113-1130.

83. A. Wikstrom, P. Gudmundson, *Acta Mater.* 2000, 48 (10): 2429-2434.

84. D. H. Zhang, Z. Q. Liu, C. Li, T. Tang, X. L. Liu, S. Han, B. Lei, C. W. Zhou, *Nano Lett.* 2004, 4 (10): 1919-1924.

85. S. H. Jo, D. Banerjee, Z. F. Ren, *Appl. Phys. Lett.* 2004, 85 (8):1407-1409.

86. Z. H. Zhong, D. L. Wang, Y. Cui, M. W. Bockrath, C. M. Lieber, *Science* 2003, 302 (5649): 1377-1379.

87. M. G. Ancona, S. E. Kooi, W. Kruppa, A. W. Snow, E. E. Foos, L. J. Whitman, D. Park, L. Shirey, *Nano Lett.* 2003, 3 (2): 135-138.

88. M. S. Arnold, P. Avouris, Z. W. Pan, *J. Phys. Chem. B* 2003, 107 (3): 659-663.

89. E. Comini, G. Faglia, G. Sberveglieri, *Appl. Phys. Lett.* 2002, 81 (10): 1869-1871.

90. Q. Kuang, C. S. Lao, M. C. Park, Y. L. Deng, A. K. Sood, D. L. Polla, Z. L. Wang, *J. Am. Chem. Soc.* 2007, 129 (19): 6070-6073.

91. X. D. Bai, P. X. Gao, Z. L. Wang, *Appl. Phys. Lett.* 2003, 82 (26): 4806-4808.

92. W. L. Hughes, Z. L. Wang, *Appl. Phys. Lett.* 2003, 82 (17): 2886-2888.

93. X. D. Wang, J. H. Song, L. Liu, *Science* 2007, 316 (5821): 102-105.

94. Z. L. Wang, J. H. Song, *Science* 2006, 312 (5771): 242-246.

95. J. H. Song, J. Zhou, Z. L. Wang, *Nano Lett.* 2006, 6 (8): 1656-1662.

96. M. Law, L. E. Greene, J. C. Johnson, R. Saykally, P. Yang, *Nat. Mater.* 2005, 4 (6):455-459.

97. J. B. Baxter, E. S. Aydil, *Appl. Phys. Lett.* 2005, 86 (5): 053114.

98. T. J. Hsueh, C. L. Hsu, S. J. Chang, P. W. Guo, J. H. Hsieh, I. C. Chen, *Scripta Mater.* 2007, 57 (1):53-56.

99. J. Cui, U. J. Gibson, *J. Phys. Chem. C* 2010, 114 (14):6408-6412.

100. K. Wang, J. Chen, W. Zhou, Y. Zhang, Y. Yan, J. Pern, A. Mascarenhas, *Adv. Mater.* 2008, 20 (17):3248-3253.

101. A. Shah, P. Torres, R. Tscharner, N. Wyrsch, H. Keppner, *Science* 1999, 285 (5428): 692-698.

102. M. A. Green, *Sol. Cells* 1982, 7 (3): 337-340.

103. B. P. Rai, *Sol. Cells* 1988, 25 (3): 265-272.

104. P. M. Jones, J. A. May, J. B. Reitz, E. I. Solomon, *J. Am. Chem. Soc.* 1998, 120 (7):

1506-1516.

105. A. E. Rakhshani, *Solid-State Electron.* 1986, 29 (1): 7-17.

106. H. Tanaka, T. Shimakawa, T. Miyata, H. Sato, T. Minami, *Appl. Surf. Sci.* 2005, 244 (1-4):568-572.

107. J. Kata, K. I. Yama, M. Matsuoka, J. Tamaki, *J. Appl. Electrochem.* 2004, 34 (7): 687-692.

108. T. Minami, T. Miyata, K. Ihara, Y. Minamino, T. Satoshi, *Thin Solid Films* 2006, 494 (1-2): 47-52.

109. J. Katayama, K. Ito, M. Matsuoka, J. Tamaki, *J. Appl. Electrochem.* 2004, 34 (7): 687-692.

110. M. Izaki, K. Mizuno, T. Shinagawa, M. Inaba, A. Tasaka, *J. Electrochem. Soc.* 2006, 153 (9): C668-C672.

111. W. M. Sears, E. Fortin, J. B. Webb, *Thin Solid Films* 1983, 103 (3): 303-309.

112. J. Herion, E. A. Niekisch, G. Scharl, *Sol. Energy Mater.* 1980, 4 (1): 101-112.

113. L. Papadimitriou, N. A. Economou, D. Trivich, *Sol. Cells* 1981, 3 (1): 73-80.

114. B. M. Kayes, H. A. Atwater, N. S. Lewis, *J. Appl. Phys.* 2005, 97 (11): 114302.

115. E. C. Garnett, P. J. Yang, *Am. Chem. Soc.* 2008, 130 (29): 9224-9227.

116. B. Tian, X. Zheng, T. J. Kempa, Y. Fang, N. Yu, G. Yu, J. Huang, C. M. Lieber, *Nature* 2007, 449 (7164): 885-888.

117. Y. Zhang, L. W. Wang, A. Mascarenhas, *Nano Lett.* 2007, 7 (5): 1264-1269.

118. J. A. Assimos, D. Trivich, *J. Appl. Phys.* 1973, 44(4):1687-1693.

119. J. A. Switzer, B. M. Manue, E. R. Raub, E.W. Bohannan, *J. Phys. Chem. B* 1999, 103 (3): 395-398.

120. E. W. Bohannan, L. Y. Huang, F. S. Miller, M. G. Shumsky, J. A. Switzer, *Langmuir* 1999, 15 (3): 813-818.

ACKNOWLEDGEMENTS

First and foremost, I would like to express heartfelt gratitude and thanks to my advisor, Prof. Ju, who has been an unwavering source of encouragement, help and support during the entire course of this work. He has been an outstanding mentor and coach throughout my PhD, which has greatly benefited me technically and otherwise. His encouragement and enthusiasm in scientific research have been a great motivation for growing and developing my research skills and scientific horizons. From him, I have learned the ways to create ideas, to organize research and to present results, which will greatly benefit me in my future career.

I would like to give my deeply heartily thanks to Prof. Nobutada Ohno and Prof. Masumi Saka. Thanks them very much for all precious advice and suggestions on my research.

Then I would also like to thank Prof. Yasuyuki Morita and Prof. Atsushi Hosoi for providing me advice and warm help throughout the course of this research.

I would also like to thank Dr. Chen for his collaboration and guidance during this work, whose constructive criticism and suggestions have been invaluable to my research.

A special note of thanks goes to all my officemates for being such excellent support during my PhD research. I hope to return the favor one day.

I want to give my sincere thanks to all the people that contributed to the development

of this work.

Finally, I am grateful to my family for their calm optimism and constant backing throughout my career and education. But for the benefit of their unshakable support, love constant championing, I would be nowhere. I cannot thank them enough for all that they've given to my life. My everlasting gratitude to my beloved husband for being my bedrock and the most enthusiastic supporter could ever hope for. His love and care warm me and make me feel strong.

Yumei YUE

Nagoya University

January 2012, Japan